ACS Energy LETTERS

http://pubs.acs.org/journal/aelccp

Incidental and Intentional Transformation: Transition Metal Pnictide and Chalcogenide Electrocatalysts for Alkaline Hydrogen Evolution

Focus Review

Kenta Kawashima, Antony Elvin Fernando Milton, John S. Archer, Daniel T. Collins, Nicolas Lorenzo Serrat, Chikaodili E. Chukwuneke, Raul A. Marquez, Lettie A. Smith, and C. Buddie Mullins*

Cite This: *ACS Energy Lett.* 2024, 9, 6126−6143

Read Online

ACCESS | Metrics & More | Article Recommendations | Supporting Information

ABSTRACT: **Transition metal pnictides and chalcogenides (X-ides) have been studied as promising electrocatalysts for the alkaline hydrogen evolution reaction (HER). These materials often undergo dynamic transformations, either on their surface or within their bulk, occurring "incidentally" during the HER or "intentionally" through electrochemical activation. Current research shows that X-ides can remain unchanged, undergo oxidation or reduction, or transform into different X-ides with reduced X-ogen (i.e., chalcogen or pnictogen) to metal ratios compared to their original forms. In this Focus Review, we explore examples of these transformations for incidental and intentional cases, identify gaps in current knowledge, discuss divergent views on the nature of catalytically active species, and provide recommendations for more accurate identification of the active HER species in future studies.**

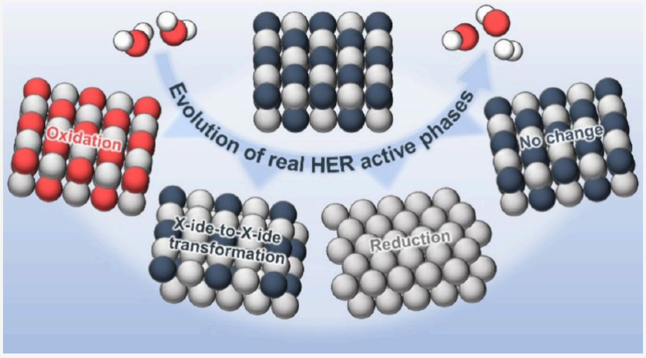

Numerous industries heavily rely on finite fossil fuels, highlighting the pressing necessity for a sustainable energy alternative. Green hydrogen, generated via renewable energy-driven electrochemical overall water splitting, emerges as a promising solution.[1−3] Despite their longstanding presence, water electrolyzers still necessitate significant enhancements to yield efficient, cost-effective, and eco-friendly hydrogen production from water.[4−6] Among the viable options, alkaline water electrolysis (AWE) stands out as one of the most advanced and economical, achieving efficiencies of up to 60% at a production cost of approximately \$5.50 kg^{-1} H_2.[2] Nevertheless, substantial strides are crucial to meet the ambitious target of \$1.00 kg^{-1} H_2 by 2031 set by the U.S. Department of Energy.[5,7−9] Despite the lagging efficiency compared to the classic, acidic counterpart proton exchange membrane water electrolysis (PEMWE),[10] AWE offers superior material compatibility:[11,12] alkaline media is much more friendly with materials than other media, offering a longer electrolyzer lifetime (i.e., AWE: 10 years; PEMWE: 3−4 years).[10] This attribute expands the scope of electrocatalyst design, leveraging a broad array of materials from the periodic table, thereby enhancing tunability for improving electrolyzer efficiency and further prolonging electrolyzer lifespan. Notably, in this pursuit, transition metal pnictides and chalcogenides (X-ides, X = N, P, As, S, Se, Te) emerge as promising groups of electrocatalytic materials for the hydrogen evolution reaction [HER: $4H_2O + 4e^- \rightarrow 2H_2 + 4OH^-$, $E° = -0.83$ V vs the standard hydrogen electrode (SHE)] and the oxygen evolution reaction (OER: $4OH^- \rightarrow O_2 + 2H_2O + 4e^-$, $E° = 0.40$ V vs SHE) in alkaline media.[13−21] Thus, far, for alkaline OER, it is well-known that most materials in these material groups

Received: August 9, 2024
Revised: October 31, 2024
Accepted: November 22, 2024
Published: December 2, 2024

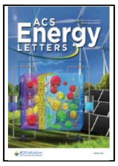

https://doi.org/10.1021/acsenergylett.4c02182

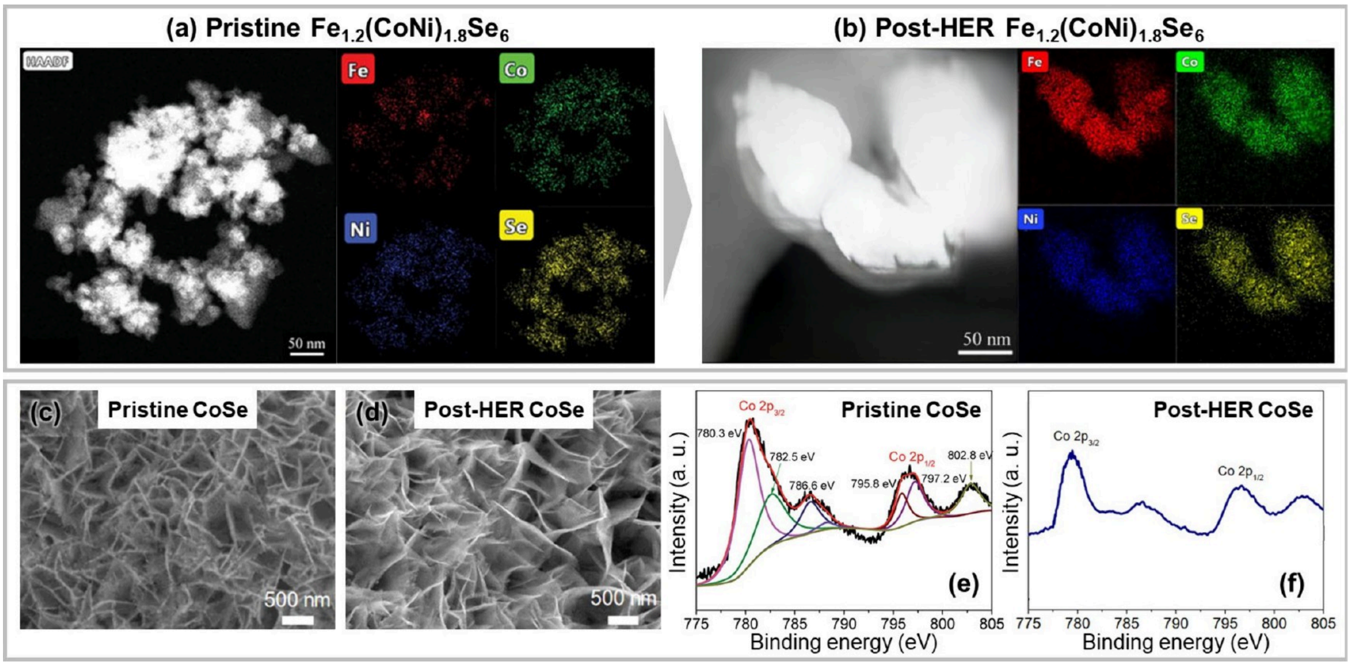

Figure 1. HAADF-STEM and corresponding elemental mapping images of $Fe_{1.2}(CoNi)_{1.8}Se_6$ nanoparticles (a) before and (b) after the HER stability test. Reprinted with permission from ref 48. Copyright 2023 Wiley. SEM images of CoSe nanowalls coated on Ni mesh (c) before and (d) after the HER testing. Co 2p XPS spectra of CoSe nanowalls coated on Ni mesh (e) before and (f) after the HER. Reprinted with permission from ref 46. Copyright 2016 Royal Society of Chemistry.

experience phase transformation (as typified by oxidation) into OER active phases [most likely their oxide/(oxy)hydroxide counterparts] due to their low thermodynamic stabilities.[17,19,22−28] Our group recently performed a comprehensive literature review, analyzing more than 890 peer-reviewed research papers on transition metal borides, carbides, pnictides, and chalcogenides.[19] Our findings indicate that approximately 87% of the well-studied transition metal pnictides and chalcogenides exhibit characteristics of "precatalysts" (precursors to true catalysts)[22] that eventually undergo phase transformations during the OER. On the other hand, previous reports have noted that transition metal X-ides also experience phase transformations during alkaline HER.[29−31] This notion is further supported by recent research articles.[32−35] Nonetheless, the comprehension of these phase transformations remains incomplete, indicating a necessity for a more systematic understanding within this field.

In this Focus Review, we contribute to the systematic understanding of the phase transformations of the transition metal pnictides (i.e., nitrides, phosphides, and arsenides) and chalcogenides (i.e., sulfides, selenides, and tellurides) known to be active electrocatalysts for alkaline HER. Specifically, representative examples (i.e., well-investigated, published studies including a sufficient amount of *in situ* and pre- and post-HER characterization data) are collected and classified into "incidental" and "intentional" transformations. Here, incidental transformation refers to a phenomenon where the material unintentionally undergoes a phase change during alkaline HER. Intentional transformation involves an electrochemical modification of electrocatalysts to improve their HER performance, which may include phase/structural transformations through techniques such as anodic/cathodic linear sweep voltammetry (LSV), cyclic voltammetry (CV), chronoamperometry (CA), or chronopotentiometry (CP), collectively referred to as electrochemical activation,[36−40,33,35,41] electroactivation,[42] or electrochemical (pre)treatment.[43,44] Furthermore, within each category (i.e., incidental/intentional transformation), the transformation cases are classified into four different main groups: (i) no transformation (Section 1.1), (ii) oxidation of metal X-ide into metal oxide/hydroxide (Section 1.2 and 2.1), (iii) transformation of metal X-ide into another metal X-ide (e.g., $NiSe_2$ → $NiSe_{1.5}$ → NiSe)[45] (Sections 1.3 and 2.2), and (iv) reduction of metal X-ide into metal (Sections 1.4 and 2.3). Here, we will also discuss any issues that need to be resolved in the future for each transformation case as necessary. In Section 3, we will introduce a few exceptional cases regarding metal X-ide crystallinity alternation: the transformation of amorphous metal X-ide into crystalline metal X-ide.[39,42] Showcasing and categorizing these transformation cases offer valuable insights to researchers in this field, aiding in uncovering the real HER active phases and understanding the alkaline HER mechanisms in electrocatalytic materials of interest. In Section 4, we will examine the thermodynamics and kinetics of phase transformations in metal X-ides during the HER in alkaline media. We will propose a generalized model for the transformation behavior of metal X-ides as alkaline HER electrocatalysts while highlighting a few key challenges that remain in this field. In closing, Section 5 offers both a summary along with recommendations for future studies.

1. INCIDENTAL TRANSFORMATION

This section describes the incidental transformation of transition metal X-ides under alkaline HER. We will present the four transformation cases (Sections 1.1−1.4) mentioned earlier and provide a couple of representative examples for each case.

1.1. No Transformation. In this group, the transition metal X-ides serve as the active catalysts for alkaline HER and remain unchanged throughout the reaction.[46−51] In general, the stability of an electrocatalyst is assessed through extended tests for alkaline HER, employing electrochemical methods such as multiscan CV, CA, and CP. Researchers commonly interpret minimal performance degradation throughout these tests as an indicator of stability in their electrocatalytic materials. Recent studies on metal X-ides, including electrodeposited Ni_3P,[52] electrodeposited amorphous MoCoNiS,[53] electrodeposited $CoSe_2$,[54] electrodeposited amorphous Ni−Se−C,[55] electrodeposited $Cu_2Se/CoSe_2$ composite,[56] Cu−Ni selenide,[49] Fe−Ni-doped metal−organic framework (MOF) derived $CoSe_2$,[51] and Ni−Fe−P−Se composite,[50] have applied similar stability evaluation methods and generally found these electrocatalysts to be stable. However, it is critical to distinguish between electrochemical and chemical stability, as these are not identical. Figure S1 displays a Pourbaix diagram for Ni_3P, selected as a representative example among these samples. Using data from the Materials Project (open-access database: https://materialsproject.org/), the diagram indicates that Ni_3P may transform into Ni metal under HER potentials and alkaline conditions (approximately pH 14). This highlights the importance of thorough material characterization before and after HER testing to accurately assess the material's stability for alkaline HER. In well-documented studies, researchers often employ techniques such as X-ray diffraction (XRD), electron microscopy [e.g., scanning electron microscopy (SEM), transmission electron microscopy (TEM)], energy-dispersive X-ray spectroscopy (EDX), and X-ray photoelectron spectroscopy (XPS) for post-HER characterization. For instance, Hu et al. demonstrated the "excellent" stability of Cu-doped ZnSe nanoparticles incorporated into N-doped carbon as catalysts for alkaline HER, substantiated by a 2000-cycle stability test followed by SEM and XRD analyses.[47] Similarly, Wu et al. confirmed the "outstanding" stability of $Fe_{1.2}(CoNi)_{1.8}Se_6$ through a 24 h CA test, complemented by subsequent high-angle annular dark-field scanning TEM (HAADF-STEM) and EDX analyses (see Figures 1a and b).[48] However, in the above examples, SEM and low-resolution STEM only offer morphological insights, and XRD and EDX provide bulk structural and compositional analyses, respec-

> Instead, it is preferable to meticulously analyze any post-HER metal X-ides, employing a comprehensive array of material characterization techniques.

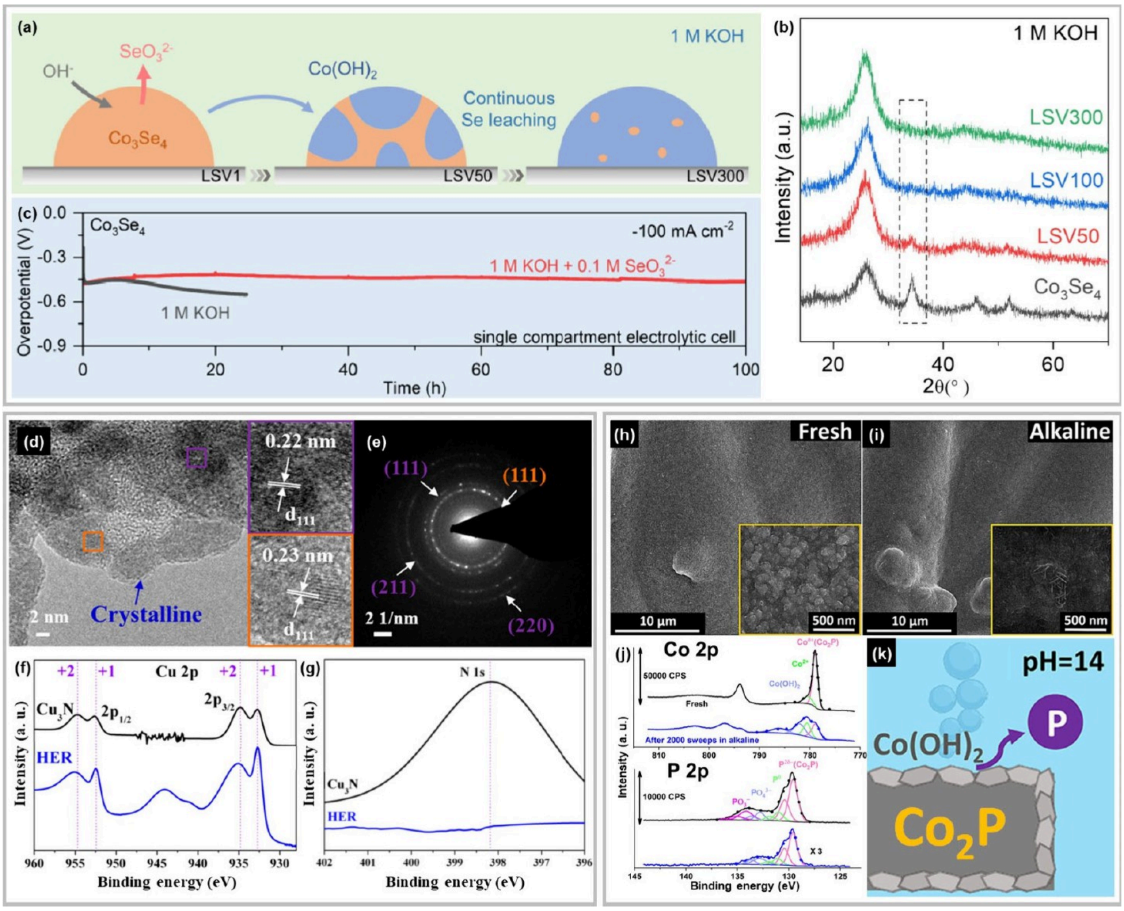

Figure 2. (a) Schematic illustration and (b) XRD patterns of Co_3Se_4 on carbon cloth after HER LSV sweeps with varying numbers of sweeps. (c) Chronopotentiometry plots of Co_3Se_4 in the presence/absence of SeO_3^{2-}, under a cathodic current density of 100 mA·cm^{-2}. Reprinted with permission from ref 69. Copyright 2023 Elsevier. (d) TEM images and (e) SAED pattern of post-HER Cu_3N (violet: Cu_3N; orange: CuO). (f) Cu 2p and (g) N 1s XPS spectra of Cu_3N before and after the HER. Reprinted with permission from ref 61. Copyright 2019 American Chemical Society. SEM images of Co_2P on carbon paper (h) before and (i) after HER testing (i.e., 2000 LSV sweeps). (j) Co 2p and P 2p XPS spectra of Co_2P before and after HER testing. (k) Schematic illustration of Co_2P during alkaline HER testing. Reprinted with permission from ref 60. Copyright 2018 American Chemical Society.

tively. In addition, quantitative analysis results for EDX are lacking.[48] Surface-sensitive analyses such as XPS and high-resolution TEM (HRTEM) are also necessary to validate assertions on high stability. Here, we provide an additional example showcasing more comprehensive characterization results for a post-HER electrocatalyst. Li et al. conducted SEM (Figures 1c and d), XRD (not shown here), and XPS analyses (Figures 1e and f) on CoSe nanowalls coated on Ni mesh before and after a 24 h overall water splitting (OWS) CA test.[46] Based on their findings, they concluded that the electrocatalyst remained stable under the tested conditions. However, a closer examination of Figures 1e and f reveals a notable decrease in peak intensity for the Co $2p_{3/2-1/2}$ doublet at around 782.5 and 797.2 eV after the 24 h OWS test, but post-HER XPS results for Se are not available. Furthermore, Figure S2 shows a Pourbaix diagram for CoSe, implying instability of CoSe under HER potentials and alkaline conditions (pH ∼ 14). Consequently, the high stability of CoSe under alkaline HER conditions remains questionable. Incidentally, Pourbaix diagrams of various metal X-ides from the Materials Project suggest instability under alkaline HER conditions for many metal X-ides. We contend that with rare exceptions [e.g., ZnSe (see Figure S3)], almost all metal X-ides may undergo some degree of phase transformation during the alkaline HER operation. Notably, the overarching lesson derived from the examples mentioned above, along with the computational insights from the Materials Project, emphasizes the importance of avoiding hasty conclusions. Instead, it is preferable to meticulously analyze any post-HER metal X-ides, employing a comprehensive array of material characterization techniques. This includes the integration of both bulk and surface-sensitive analyses, facilitating the more accurate identification of their true stability.[31]

1.2. Oxidation of Metal X-ide into Metal Oxide/Hydroxide. Numerous X-ides reported to date belong to this group. These transition metal X-ides undergo surface or bulk reconstruction, such as partial oxidation[57−66,32,21,67] or complete oxidation,[68,69,34] into their oxide or hydroxide forms during the alkaline HER process. In the case of complete oxidation, the resultant oxide/hydroxide species serve as the actual active sites for the HER. For example, research conducted by the Chakraborty and Zhang groups demonstrated that sulfide materials, specifically crystalline Cu_9S_5[34] and amorphous $CoNiS_x$,[68] undergo oxidation to form their corresponding oxides (crystalline Cu_2O with amorphous CuO and crystalline Ni- and S-codoped CoO, respectively) along with surface sulfate species under their specific HER conditions. As shown in Figures 2a−c, Jiang et al. synthesized crystalline Co_3Se_4 on carbon cloth and conducted multiple HER LSV sweeps (ranging from 0 to 300) to monitor its phase transformation.[69] In the XRD analysis, the intensity of the diffraction peaks corresponding to Co_3Se_4 significantly decreased with increasing LSV sweeps (see Figure 2b). Simultaneously, the selenium content in the Co_3Se_4 electrocatalyst decreased, while its concentration in the electrolyte increased, as confirmed by XPS and inductively coupled plasma-mass spectrometry (ICP-MS). Furthermore, $Co(OH)_2$ formation was validated by XPS, Raman spectroscopy, and TEM after 300 LSV sweeps. These observations suggest that crystalline Co_3Se_4 was almost entirely converted to low-crystallinity $Co(OH)_2$ after 300 LSV sweeps (Figure 2a). Additionally, XPS (Se 3p region) and Auger electron spectroscopy (not shown here) confirmed that there were almost no Se−O species on the post-HER electrocatalyst surface.

In the case of partial oxidation, two scenarios can be considered based on the extent of electrocatalyst surface oxidation: (i) complete surface oxidation[57,59,61,64,21] and (ii) partial surface oxidation.[58,60,62,65,32] Similar to the case of complete oxidation (i.e., bulk reconstruction), when the X-ide electrocatalyst surface is entirely oxidized into the corresponding oxide/hydroxide, the resulting oxide/hydroxide can be considered the dominant HER active phase. The Driess group conducted XRD, TEM, and XPS analyses on post-HER Cu_3N to investigate its transformation during the HER process.[61] The XRD pattern confirmed the preservation of Cu_3N and the formation of crystalline CuO. As shown in Figures 2d and e, TEM analysis revealed the formation of crystalline Cu_3N@CuO core@shell structures. XPS results indicated the presence of Cu^{2+} and Cu^+ signals, corresponding to CuO and Cu_3N, respectively, in the post-HER sample (Figure 2f). However, the N signal was absent after the HER, possibly due to the formation of a thick CuO shell, suggesting complete surface oxidation (Figure 2g). Additionally, the observation of a cathodic peak related to the reduction of higher oxidation state Cu species to metallic Cu in the HER LSV led the authors to hypothesize that surface crystalline CuO may form through the generation of metallic Cu on the surface of Cu_3N under reductive potentials, followed by oxidation in a strong alkaline medium or instantaneous aerial oxidation when removed from the electrolyte. The Driess group also suggested similar post-HER surface oxidation behaviors for the $FeSe_2$ and Ni_xP_y ($Ni_{12}P_5$ and Ni_2P) systems.[58,59] The issues concerning post-HER oxidation will be discussed in detail later in this section and Sections 1.4 and 2.3. The Liu lab[57] and the Manna lab[21] examined other pnictides, such as a Ni−P composite (Ni_5P_4, Ni_2P, and NiP_2) and NiAs. They found that these nickel pnictides underwent nearly complete surface oxidation into amorphous nickel hydroxide, along with phosphate and arsenic oxide, after long-term HER testing, respectively. On the other hand, in partial surface oxidation, both as-formed oxide/hydroxide and X-ide species can coexist on the post-HER electrocatalyst surface, possibly participating in the HER process. As revealed by Zhang et al.,[60] Co_2P on carbon paper experienced surface partial oxidation into $Co(OH)_2$ after 2000 HER LSV sweeps (see Figures 2h−k). The surface morphology shows minimal changes in the low-magnification SEM images of the pre- and post-HER samples (Figures 2h and i). However, in the high-magnification SEM images (insets of Figures 2h and i), flake-like nanostructures appeared on the post-HER electrocatalyst surface, indicating the formation of $Co(OH)_2$.[70] The pre- and post-HER XPS results are shown in Figure 2j. XPS-based quantitative analysis reveals that the surface composition ratio of $Co^{\delta+}$ ($0 < \delta < 1$), associated with Co_2P, decreased from 4 to 0.5. This indicates that approximately 60% of the surface Co_2P species in the original sample underwent oxidation into $Co(OH)_2$ and oxidized surface P species, likely PO_4^{3-}, during HER testing. Importantly, the XPS peak intensity of P species decreased drastically after the HER, with soluble PO_3^- components nearly disappearing, suggesting selective dissolution of phosphorus (see Figure 2j). The Liu lab[62] and our lab[24] investigated Co−P composite (CoP_2, CoP, and Co_2P) and amorphous Ni−P HER electrocatalysts, respectively. Both systems exhibited similar partial surface oxidation, leading to the formation of cobalt oxide/hydroxide with phosphate

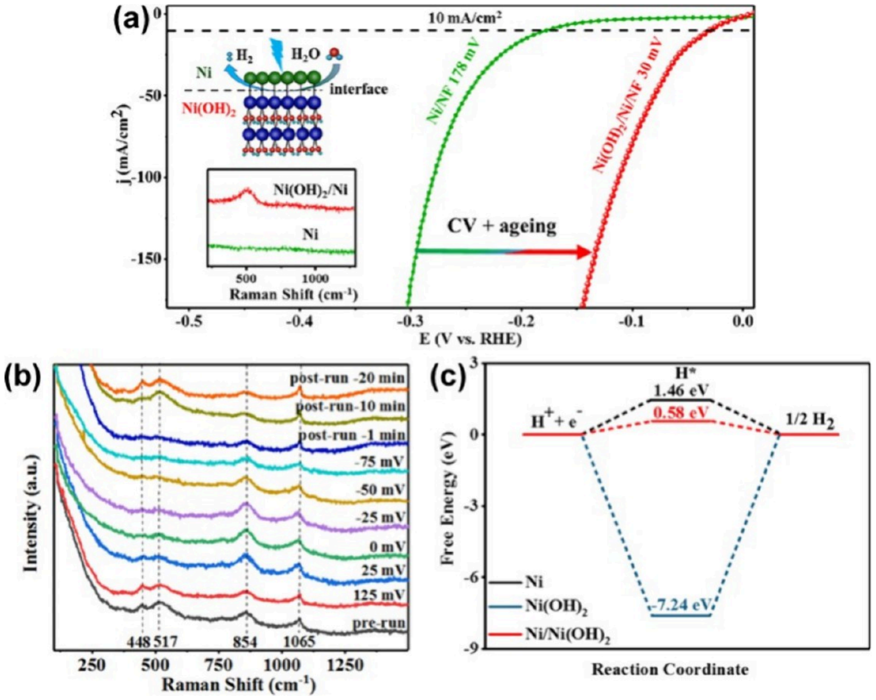

Figure 3. (a) Linear sweep voltammograms of Ni nanoclusters deposited on Ni foam (Ni/NF) and activated Ni/NF [$Ni(OH)_2/Ni/NF$], which contains $Ni/Ni(OH)_2$ heterostructures, in alkaline media (1 M KOH). (b) *In situ* Raman spectra of $Ni(OH)_2/Ni/NF$ collected at various potentials (125 to −75 mV vs RHE) in 1 M KOH, along with the corresponding prerun and postrun Raman spectra. (c) Calculated HER free energy pathways on Ni, $Ni(OH)_2$, and $Ni/Ni(OH)_2$ model surfaces. Reprinted with permission from ref 78. Copyright 2021 Elsevier.

species in the case of Co−P and $Ni(OH)_2$ with $Ni_3(PO_4)_2$ in the case of Ni−P. Recently, Hu et al. performed *in situ* TEM analysis on a more complex X-ide HER electrocatalyst, specifically Ru-doped $NiPS_3$ (Ru-$NiPS_3$) nanosheets (NSs).[32] Their findings revealed that amorphization (partial oxidation) occurred at the edges of the Ru-$NiPS_3$ NSs. Post-HER XPS analysis further confirmed the presence of Ni−S components and the partial and complete oxidation of Ni−S and Ni−P into Ni−O species with sulfate and sulfite, and Ni−O species with P−O species, respectively. Additionally, surface Ru^0 species were completely oxidized to Ru^{4+} species following the HER.

Moving forward, we discuss three primary concerns related to X-ide electrocatalysts undergoing oxidation during the HER process. (i) First, it is important to understand the roles of oxidized chalcogen/pnictogen species (i.e., oxyanions) in the HER process. As noted in the above-mentioned examples, most X-ides exhibit oxyanion species after the HER. However, the impact of these oxyanions on the resulting HER activity remains unclear. Here, we will review several studies that provide insights into the effect of these oxyanions on HER activity. As discussed earlier, the study by Jiang et al. revealed that during the alkaline HER, Co_3Se_4 transforms into $Co(OH)_2$ (i.e., hydroxylation), accompanied by continuous leaching of selenium into the electrolyte (Figure 2a).[69] They also discovered that the electrochemical stability of Co_3Se_4 deteriorated during long-term HER testing due to selenium leaching and excessive hydroxylation (Figure 2c). To address this issue, SeO_3^{2-} was added to the electrolyte to establish a new equilibrium of selenium at the electrocatalyst/electrolyte interface, thereby preventing selenium leaching and enhancing the electrochemical stability of Co_3Se_4 (see Figure 2c). This study implies that the electrochemical stability of transition metal X-ides may generally vary depending on the absolute amount of electrolyte when testing these materials in a batch electrochemical cell. Incidentally, note that in a single-compartment batch electrolyzer, oxyanions generated from the cathode can also alter the chemical environment around the anode.[71,72,69] Notably, Walter et al. studied elemental chalcogens (sulfur, selenium, and tellurium) electrophoretically deposited on Ni foam for alkaline HER, where they exhibited HER activity.[73] Selenium demonstrated superior performance compared to sulfur and tellurium, with HER overpotentials (η_{10}) of 105 ± 2, 193 ± 5, and 274 ± 3 mV at -10 mA·cm^{-2} in 1 M KOH for Se, S, and Te, respectively. After long-term HER testing, selenium and sulfur underwent partial surface oxidation, forming SeO_2 and S^{6+} species (likely SO_4^{2-}), respectively, while tellurium experienced complete surface oxidation to TeO_2. Furthermore, all three chalcogens experienced dissolution into the electrolyte, with the dissolved quantities in the order of Te > S > Se. Despite these surface structural/compositional changes, all materials retained some level of HER activity. This study shows that chalcogen species themselves possess inherent HER activity. Additionally, during the HER, phosphate species generated from metal phosphides were believed to form a surface passivation layer.[65] This layer could have prevented the dissolution of inner/bulk phosphides and potentially increased local charge density, thereby trapping protons and enhancing the HER process.[65] Recently, the Kim group also found that forming metal phosphide/phosphate heterostructures can enhance HER performance due to their high surface area and modulated surface electronic structures.[74,75] Incidentally, in water and methanol oxidation electrocatalysts [e.g., transition metal (oxy)hydroxides], it is known that the incorporation or adsorption of oxyanions into or onto their lattice or surface can modify their electronic properties, leading to enhanced performance.[71,72] Nevertheless, the effects of oxyanions generated from X-ides on alkaline HER performance require further investigation.

(ii) Second, when discussing the mechanism of X-ides exhibiting oxidation in post-HER characterizations, it is crucial to consider the timing of X-ide oxidation—whether it occurred during the HER process or after HER testing. This distinction is crucial for accurately delineating the HER mechanism of metal X-ides. As discussed above, the Driess group observed the complete surface oxidation of Cu_3N to $Cu(OH)_2$ through post-HER characterizations.[61] They hypothesized that Cu_3N might undergo *in situ* reduction to metallic Cu under HER potentials, with $Cu(OH)_2$ subsequently forming from the resulting oxidation of metallic Cu after HER testing (i.e., post-HER oxidation). If this hypothesis holds, the metallic Cu formed *in situ* could represent the true active phase for the HER rather than $Cu(OH)_2$. This assumption implies that the presence of $Cu(OH)_2$ on the post-HER Cu_3N surface could potentially lead to misinterpretations regarding the actual active phase for the HER. Moreover, Chen et al. conducted both *ex situ* and *in situ* characterizations of Ni/Ni_xP composite HER electrocatalysts grown on carbon cloth ($Ni/Ni_xP/CC$), observing similar oxidation after the HER process.[76] *Ex situ* characterizations indicate that the $Ni/Ni_xP/CC$ electrode underwent significant morphological and compositional surface changes, including complete surface oxidation and phosphorus leaching, resulting in the formation of amorphous $Ni(OH)_2$ after alkaline HER testing. However, *in situ* Raman spectroscopy revealed that these surface reconstructions did not occur during the HER process. Instead, *in situ* Raman spectroscopy suggested that the negatively charged phosphorus ions might be the catalytically active species, attracting the positively charged protons necessary for the HER. This finding suggested that the surface amorphous $Ni(OH)_2$ formed as a result of post-HER oxidation and did not contribute to the resulting HER activity. These examples highlight the importance of combining *ex situ* and *in situ* characterizations to accurately identify the active phases in X-ide electrocatalysts for future research.

(iii) Finally, one must ascertain whether the metal oxide/hydroxide species generated *in situ* during/after the HER can remain stable and act as catalytically active species under HER potentials. We so far reviewed several cases where metal X-ides completely/partially transformed into their oxide/hydroxide counterparts such as CuO, $Ni(OH)_2$, $Co(OH)_2$, etc. The Pourbaix diagrams for these compounds, shown in Figures S4−6, indicate that these oxide/hydroxide compounds can be reduced to their metal counterparts under HER potentials. Furthermore, a few studies on transition metal hydroxide electrocatalysts for alkaline HER have also observed their reduction into corresponding metals through *in situ* Raman spectroscopy.[77−79] For instance, Faid et al. found that both α-$Ni(OH)_2$ and β-$Ni(OH)_2$ can be reduced into Ni under the HER potentials in alkaline media.[77] More recently, Lai et al. fabricated a $Ni/Ni(OH)_2$ heterostructure on Ni foam [$Ni/Ni(OH)_2/NF$] using cyclic-voltammetric treatment followed by aging of Ni nanoclusters that were electrochemically deposited on Ni foam (Ni/NF).[78] This heterostructure was evaluated for its alkaline HER performance and examined by *in situ* Raman spectroscopy. As illustrated in Figure 3a, $Ni/Ni(OH)_2/NF$ outperformed Ni/NF for the HER. Both prerun, *in situ*, and postrun Raman spectroscopy results showed four peaks at 448, 517, 854, and 1065 cm^{-1}, corresponding to the A_{1g} lattice mode of β-$Ni(OH)_2$, the second-order acoustic mode of β-$Ni(OH)_2$, the ν_2 vibrational mode of NO_3^- (from the synthesis)/E_g O−H bending mode of β-$Ni(OH)_2$, and the ν_1 vibrational mode of NO_3^-, respectively (see Figure 3b).[80] Notably, by adjusting the potential from 125 to −75 mV vs the reversible hydrogen electrode (RHE), the intensity of the characteristic peaks for β-$Ni(OH)_2$ at 448 and 517 cm^{-1} gradually decreased, indicating the partial reduction of β-$Ni(OH)_2$ to Ni metal. Furthermore, upon removal of the cathodic potentials, β-$Ni(OH)_2$ reformed on the $Ni/Ni(OH)_2/NF$ surface, indicating the short lifetime of *in situ* formed Ni metal species. This observation emphasizes the importance of using *in situ* characterization techniques to confirm the electroreduction of metal hydroxides. Moreover, Figure 3c presents density functional theory (DFT) results, displaying the hydrogen adsorption energies for Ni, $Ni(OH)_2$, and $Ni/Ni(OH)_2$ surfaces. These results confirmed that $Ni/Ni(OH)_2$ demonstrates the optimal hydrogen adsorption energy. In contrast, $Ni(OH)_2$ exhibits excessively strong binding of hydrogen intermediates. This implies that even in nickel X-ides with complete surface oxidation, the high HER activity could be attributed to the presence of the $Ni(OH)_2$ and *in situ* formation of Ni metal heterointerfaces, which serve as the dominant active sites for the HER. In addition to the examples regarding nickel hydroxides, Jiang et al. argued the transformation of α-$Co(OH)_2$ into metallic Co species under the cathodic potentials in alkaline media (1 M KOH) occurred based on their *in situ* Raman spectroscopy observation.[79]

Accordingly, we suggest that the electrocatalysis research community should assume that the oxide/hydroxide compounds derived from X-ides are potentially reduced to metallic species under HER conditions.

Accordingly, we suggest that the electrocatalysis research community should assume that the oxide/hydroxide compounds derived from X-ides are potentially reduced to metallic species under HER conditions. It is essential to consider the contributions of these metallic species to the resultant HER performance.

1.3. Transformation of Metal X-ide into Another Metal X-ide. In this group, during the HER process, the surface and bulk of metal X-ides transform into other metal X-ides with lower metal/X-ogen ratios through the spontaneous leaching of X-ogen (chalcogen/pnictogen) species.[45,81] Consequently, in the post-transformation electrocatalysts, the newly generated X-ides become the dominant HER active species. Currently, only a limited number of studies are available regarding various sulfides [NiS_2, α-NiS, β-NiS, Ni_3S_4, and $Ni_{1-x}Fe_xS_2$][81] and a few selenide systems ($NiSe_2$,[41,45] $Ni_{0.85}Se$,[41] and $NiSe_2/Ni_{0.85}Se$ composites[41]). Specifically, Sun et al. studied several sulfides: NiS_2, α-NiS, β-NiS, Ni_3S_4, and $Ni_{1-x}Fe_xS_2$ ($x \approx 0$ to 0.33) as alkaline HER electrocatalysts via *in situ* Raman spectroscopy, *in situ* X-ray absorption spectroscopy (XAS), and other *ex situ* characterizations. These sulfides exhibited a dynamic transformation from the surface to the bulk, driven by sulfur vacancies. As seen in Figure 4a, all tested sulfides showed the presence of the pure or Fe-incorporated Ni_3S_2 phase on their surfaces, which is the active phase for the HER. Figures 4b and c show the Raman spectra of the as-

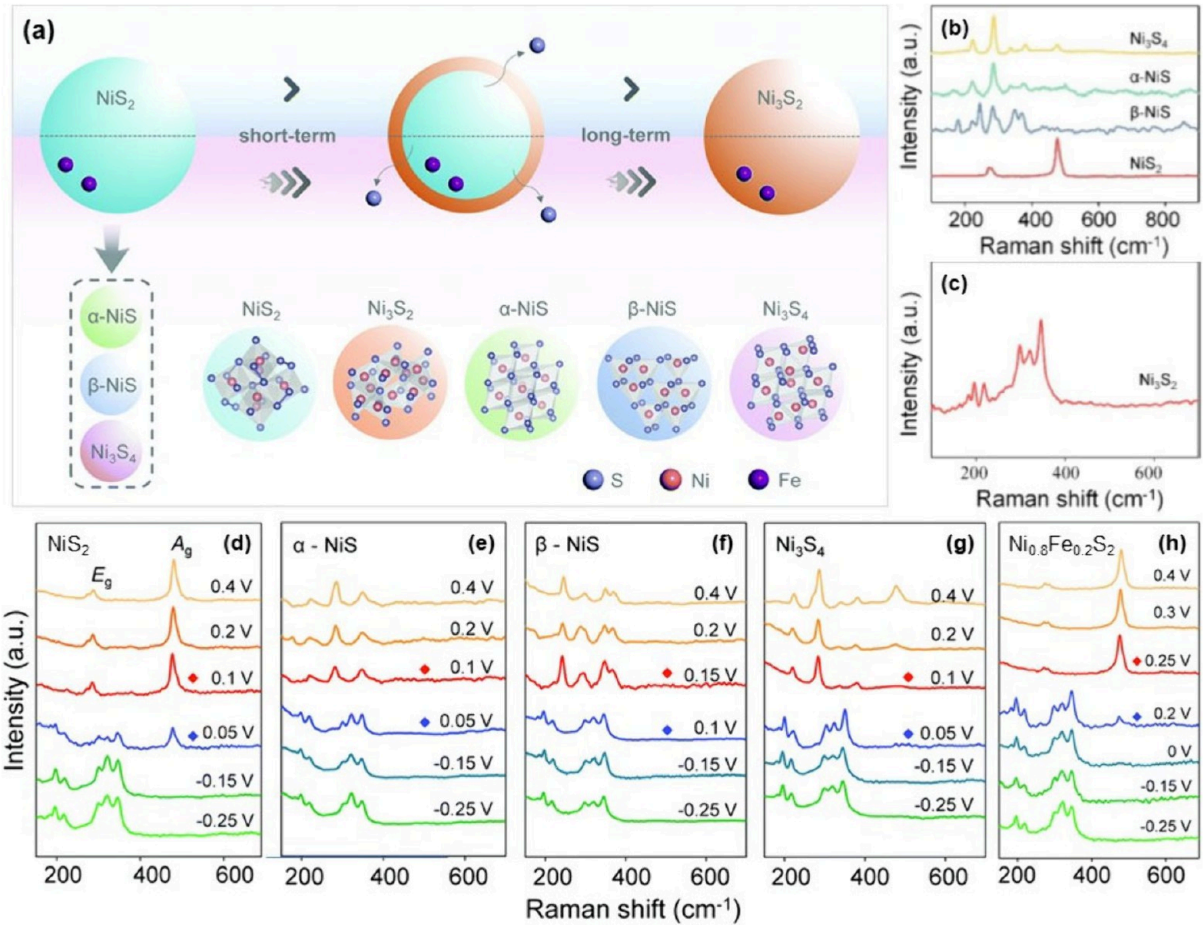

Figure 4. (a) Schematic illustration of the *in situ* phase transformation of various nickel sulfides (NiS_2, α-NiS, β-NiS, and Ni_3S_4) and iron-doped nickel sulfides [$Ni_{1-x}Fe_xS_2$ ($x \approx 0$ to 0.33)] during the alkaline HER process. Raman spectra of (b) NiS_2, α-NiS, β-NiS, Ni_3S_4, and (c) Ni_3S_2. *In situ* Raman spectra of (d) NiS_2, (e) α-NiS, (f) β-NiS, (g) Ni_3S_4, and (h) $Ni_{0.8}Fe_{0.2}S_2$ collected at various potentials (0.4 to −0.25 V vs RHE) in 1 M KOH. Reprinted with permission from ref 81. Copyright 2022 Royal Society of Chemistry.

prepared sulfides and Ni_3S_2 as reference data. Figures 4d−h display the *in situ* Raman spectroscopy results for NiS_2, α-NiS, β-NiS, Ni_3S_4, and $Ni_{0.8}Fe_{0.2}S_2$. Here, $Ni_{0.8}Fe_{0.2}S_2$ is a representative sample of $Ni_{1-x}Fe_xS_2$ ($x \approx 0$ to 0.33). As depicted in Figures 4d, e, and g, the NiS_2, α-NiS, and Ni_3S_4 samples exhibited the same applied potential threshold (0.1 to 0.05 V vs RHE) for their phase transformation into Ni_3S_2. This indicates that NiS_2, α-NiS, and Ni_3S_4 transformed into Ni_3S_2 at an applied potential of approximately 0.1 to 0.05 V vs RHE. Conversely, β-NiS displayed a higher transformation potential threshold (0.15 to 0.1 V vs RHE) (see Figure 4f), likely due to the presence of the $Ni-S_5$ motif in β-NiS, which can readily transform into the $Ni-S_4$ motif in Ni_3S_2. Additionally, compared with NiS_2, the $Ni_{1-x}Fe_xS_2$ samples showed higher transformation potential thresholds (see Figure 4h), and the transformation potential threshold range gradually shifted with increasing the Fe incorporation level ($x = 0$ to 0.2). Accordingly, the Fe incorporation reduces the energy for phase reconfiguration in $Ni_{1-x}Fe_xS_2$ electrocatalysts by increasing sulfur vacancies, as shown by X-ray absorption fine structure (XAFS) results (not shown here). This Fe-incorporation effect may aid sulfur atom removal and interdiffusion, easing the transition to the active phase (i.e., Fe-incorporated Ni_3S_2) and resulting in a higher transformation potential threshold. Note that Ni_3S_2 could potentially transform into metallic Ni at a pH of approximately 14 and under HER potentials (see Figure S7), which should be explored in future research. Similarly, the Lau group employed *in situ* Raman spectroscopy, *in situ* synchrotron XRD, and various *ex situ* characterization techniques to investigate the transformation of $NiSe_2$ during the alkaline HER.[45] Both the experimental and computational results indicated the transformation of cubic $NiSe_2$ into hexagonal NiSe (i.e., $NiSe_2 \rightarrow NiSe_{1.5} + 0.5Se \rightarrow NiSe + Se$) during the HER process. DFT calculations suggest that charge transfer occurs from the Se site to the Ni site after this phase transformation process, resulting in increased electrical conductivity and an upward shift of the d-band center (NiSe becomes the actual HER active phase). These changes are attributed to enhanced HER activity. Notably, as indicated in Figure S8, the newly formed NiSe has the potential to further transform into Se-poor nickel selenide and nickel metal (i.e., $Ni_3Se_4 + Ni_3Se_2 \rightarrow Ni_3Se_2 \rightarrow Ni$) at a pH of around 14 and under HER operating potentials, which also warrants further investigation in the future. Wu et al. also explored the behavior of $NiSe_2$, $Ni_{0.85}Se$, and $NiSe_2/Ni_{0.85}Se$ under cathodic potentials (−0.05 to −0.6 V vs RHE) in alkaline media using *in situ* Raman spectroscopy.[41] For all the selenide samples, the intensity of the peaks corresponding to A_g and T_g modes of Se−Se stretching progressively decreased with increasing the potential cathodically. The authors attributed this reduction in intensity to partial Se leaching from the selenide samples into the electrolyte. This Se leaching

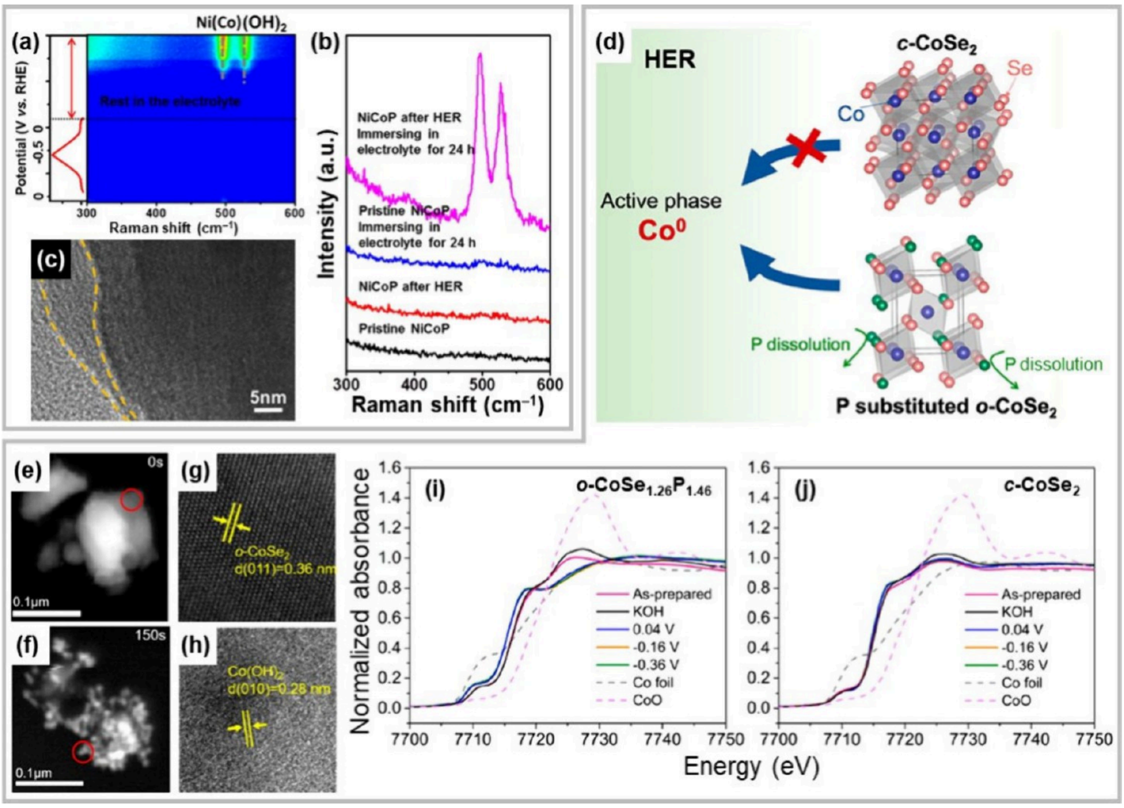

Figure 5. (a) Color-mapped profile of *in situ* Raman spectra of NiCoP during the alkaline HER. (b) Corresponding Raman spectra of pristine and post-HER NiCoP samples before and after 24 h of immersion in alkaline electrolyte. (c) TEM image of NiCoP after long-term HER testing (24 h of CP at −10 mA·cm^{-2}). Reprinted with permission from ref 82. Copyright 2020 Elsevier. (d) Schematic illustration of structural transformation of *c*-$CoSe_2$ and *o*-$CoSe_{1.26}P_{1.42}$ during the alkaline HER. *In situ* STEM images of *o*-$CoSe_{1.26}P_{1.42}$ particles immersed in the alkaline electrolyte for (e) 0 and (f) 150 s. TEM images of the selected areas of *o*-$CoSe_{1.26}P_{1.42}$ at (g) 0 and (h) 150 s. *In situ* Co K-edge XANES spectra of (i) *o*-$CoSe_{1.26}P_{1.42}$ and (j) *c*-$CoSe_2$ collected at various potentials (0.04 to −0.36 V vs RHE) in the alkaline electrolyte. Reprinted with permission from ref 83. Copyright 2019 American Chemical Society.

may induce a phase transformation (likely $NiSe_2 \rightarrow Ni_{0.85}Se \rightarrow NiSe + Ni_3Se_2$),[33,41] which will be elaborated further in Section 2.2.

1.4. Reduction of Metal X-ide into Metal.

Regardless of the conversion process, metal X-ides within this group are ultimately reduced to their metallic counterparts, accompanied by the intense leaching of X-ogen species under the HER potentials in alkaline media.[40,82,83] The *in situ* generated metal species act as active sites for the HER or at least significantly contribute to HER activity. For example, Zou et al. grew hierarchical NiCoP microflower structures on Ni foam and examined their surface reconstruction during and after the HER via *in situ*/*ex situ* Raman spectroscopy and *ex situ* TEM/XPS/ICP-optical emission spectroscopy (OES).[82] *In situ* and *ex situ* Raman spectroscopy results are shown in Figures 5a and b. Note that NiCoP and the pure Ni and Co metals do not exhibit any peaks in the 300 to 700 cm^{-1} range because NiCoP is an interstitial compound, and pure metals do not produce Raman signals. For the *in situ* Raman spectroscopy testing, an HER CV scan was performed. Initially, the electrode was immersed in the electrolyte, and no significant changes were observed (Figures 5a and b). During the HER CV scan, Raman signals were not detected (Figure 5a). Additionally, the authors performed ICP-OES analysis on two electrolyte samples: one after immersing the electrode in the electrolyte for 12 h and another after 12 h of HER testing. The post-HER electrolyte showed a higher phosphorus concentration (50 ppm) than the postimmersion sample (12 ppm), indicating greater phosphorus leaching from NiCoP under the HER process. These *in situ* Raman and *ex situ* ICP-OES results suggest the surface transformation of NiCoP into metallic Ni/Co during the HER, with the *in situ* generated Ni/Co serving as the actual active species for the HER. After conducting the HER CV scan, the electrode was left to rest in the electrolyte for a few hours (Figure 5a), including a 24 h period (Figure 5b). During this immersion period, new Raman signals appeared at 494 and 536 cm^{-1}, indicating the gradual emergence of $Ni(OH)_2$ and $Co(OH)_2$ due to post-HER surface oxidation. Additionally, *ex situ* TEM and XPS analyses confirmed the formation of a thin, amorphous layer of $Ni(OH)_2$ and $Co(OH)_2$ on the NiCoP surface (see Figure 5c). Furthermore, the post-HER NiCoP was exposed to ambient air for two days and tested for the HER again. The air-exposed sample showed a significant decline in HER activity compared to the unexposed one. This observation implies that the formation of $Ni(OH)_2$ and $Co(OH)_2$ species may obstruct the active sites for the HER. Recently, a similar post-HER oxidation phenomenon was observed in a selenide-based heterostructure composite. Guo et al. investigated the structural and compositional changes of a $Ni_3Se_4/NiSe_2$ composite under open circuit potential (OCP) and different cathodic potentials (ranging from 0 to −0.3 V vs RHE) using *in situ* Raman spectroscopy.[40] Under the OCP, the peaks corresponding to $NiSe_2$ were clearly identified. Upon applying and gradually increasing cathodic potentials, the A_g

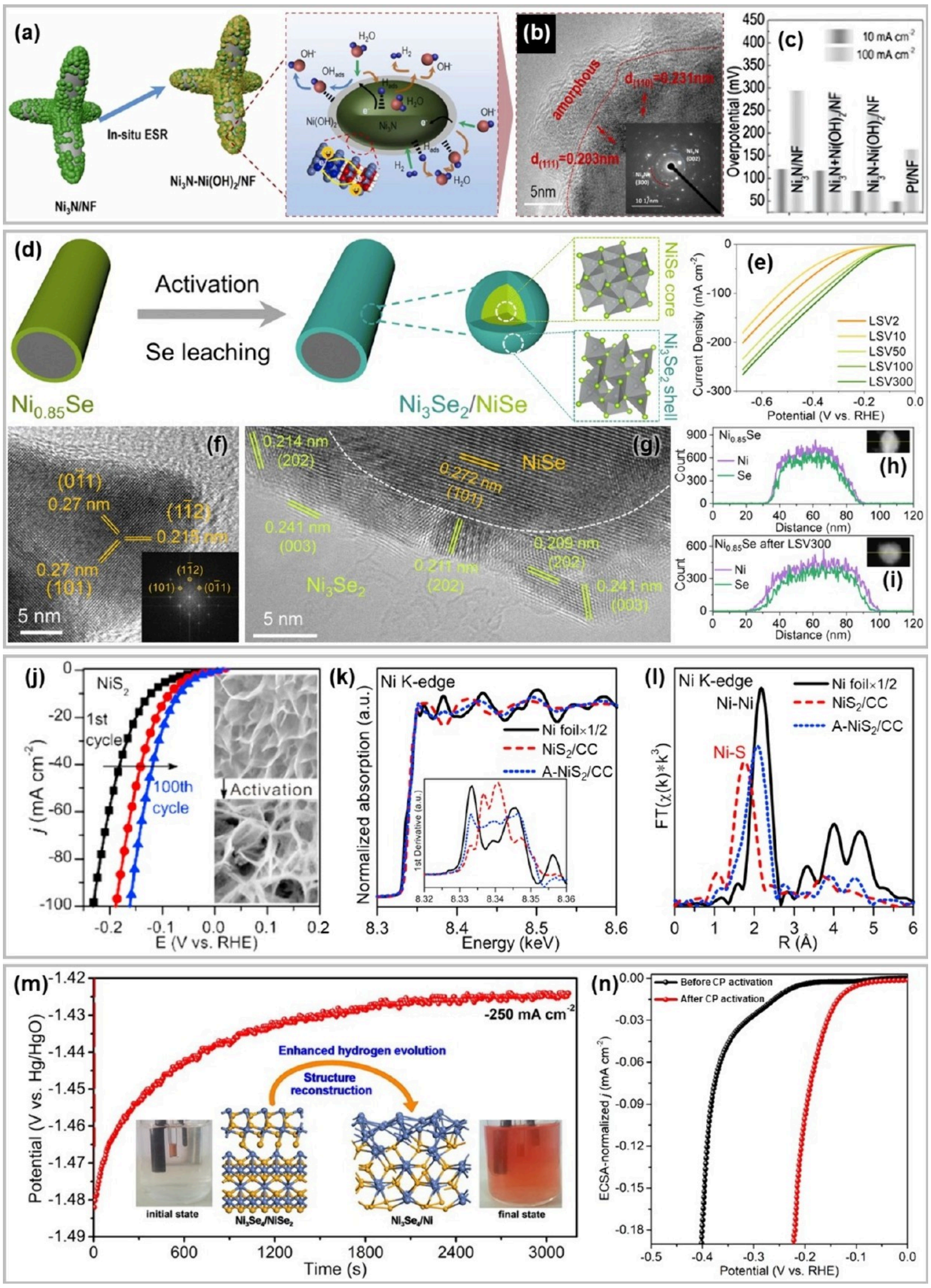

Figure 6. (a) Schematic illustration of the *in situ* electrochemical surface reconfiguration (ESR) of Ni_3N on Ni foam (Ni_3N/NF) and the alkaline HER mechanism of the resultant $Ni_3N-Ni(OH)_2$ heterostructures on Ni foam ($Ni_3N-Ni(OH)_2$/NF). (b) TEM image and corresponding SAED pattern of $Ni_3N-Ni(OH)_2$/NF. (c) Bar graph of the HER overpotentials of Ni_3N/NF, $Ni_3N+Ni(OH)_2$/NF, $Ni_3N-Ni(OH)_2$/NF, and Pt/NF at −10 and −100 mA·cm^{-2}. Reprinted with permission from ref 44. Copyright 2022 Elsevier. (d) Schematic illustration of the electrochemical activation of $Ni_{0.85}Se$. (e) Linear sweep voltammograms of $Ni_{0.85}Se$ during the activation in 1 M KOH. TEM images of $Ni_{0.85}Se$ (f) before and (g) after 300 LSV scans. EDX line-scanned elemental profiles of $Ni_{0.85}Se$ (h) before and (i) after 300 LSV scans. Reprinted with permission from ref 33. Copyright 2023 Royal Society of Chemistry and Chinese Chemical Society. (j) Linear sweep voltammograms of NiS_2 nanosheets grown on Ni foam (NiS_2/NF) during the activation in 1 M KOH. (k) *In situ* XAS, (inset) XANES, and (l) EXAFS spectra of Ni foil and NiS_2 on carbon cloth (NiS_2/CC) before and after the activation. Reprinted with permission from ref 36. Copyright 2017 Elsevier. (m) Potential vs time plot of $Ni_3Se_4/NiSe_2$ during the CP activation at a current density of −250 mA·cm^{-2} in 1 M KOH. (inset) Digital photographs of electrolyte before and after the CP activation. (n) ECSA-normalized linear sweep voltammograms of $Ni_3Se_4/NiSe_2$ before and after the CP activation. Reprinted with permission from ref 40. Copyright 2022 Elsevier.

and T_g peaks, associated with the stretching modes of Se−Se pairs, gradually decreased. At higher cathodic potentials (−0.25 and −0.3 V vs RHE), a new peak, attributed to amorphous elemental selenium, was observed. DFT calculations showed that the formation enthalpy of Ni_3Se_4 is −0.35 eV, compared to −0.29 eV for $NiSe_2$ indicating that Ni_3Se_4 is thermodynamically more stable than $NiSe_2$. Based on both experimental and computational findings, the authors proposed that $NiSe_2$ within the $Ni_3Se_4/NiSe_2$ composite could selectively transform into metallic nickel and elemental selenium. After *in* *situ* Raman spectroscopy, the sample was washed, air-dried, and tested again via *ex situ* Raman spectroscopy. Notably, along with Se−Se vibration modes from residual selenides, a broad peak for Ni−O vibrations appeared, indicating post-HER oxidation of Ni to NiO. Incidentally, similar post-HER surface oxidation behaviors for CoS_2 and Ni_2P in acidic media were recently reported by the Najafpour group.[84,85] These examples highlight the relatively short lifetime of *in situ* formed metallic species and underscore the importance of employing *in situ* characterization techniques to detect them. Additionally, when discussing the X-ide HER mechanism, it is important to consider not only post-HER oxidation but also pre-HER oxidation. Utilizing various *in situ* characterization techniques such as STEM, Raman spectroscopy, X-ray absorption near-edge structure (XANES) spectroscopy, and extended XAFS (EXAFS) spectroscopy, Zhu et al. revealed that P-substituted $CoSe_2$ with an orthorhombic crystal system (o-$CoSe_{1.26}P_{1.42}$) was converted into metallic Co under the HER potentials (see Figure 5d) through the formation of $Co(OH)_2$ via pre-HER oxidation.[83] The authors first immersed o-$CoSe_{1.26}P_{1.42}$ and $CoSe_2$ with a cubic crystal system (c-$CoSe_2$) in the KOH aqueous solution and evaluated their stability through *in situ* STEM and *ex situ* TEM (Figures 5e−h). Within 150 s, o-$CoSe_{1.26}P_{1.42}$ particles experienced drastic morphological changes, such as particle size shrinkages due to the pre-HER oxidation and subsequent phosphorus leaching. Simultaneously, the formation of many $Co(OH)_2$ nanoparticles (below 10 nm) around the particle surfaces was also confirmed (Figure 5h). In contrast, c-$CoSe_2$ exhibited no significant changes over the same period, indicating that c-$CoSe_2$ is more stable than o-$CoSe_{1.26}P_{1.42}$. The instability of o-$CoSe_{1.26}P_{1.42}$ is due to the easy leaching of P species into the alkaline electrolyte, which facilitates pre-HER oxidation. According to the *in situ* XANES results (Figures 5i and j), both o-$CoSe_{1.26}P_{1.42}$ and c-$CoSe_2$ exhibited surface oxidation when immersed in a KOH aqueous solution. Under cathodic potentials, only o-$CoSe_{1.26}P_{1.42}$ underwent significant surface reduction to metallic Co species (Figure 5i), similar to the behavior discussed in Section 1.2 (see especially Figure 3). *In situ* Raman spectroscopy further confirmed the formation of metallic Co species by showing a decrease in the intensity of peaks corresponding to $Co(OH)_2$. Additionally, *in situ* EXAFS results suggested that incorporating phosphorus creates additional vacancies or defects in the $CoSe_2$ crystal lattice, facilitating the transformation into the HER active phase (i.e., metallic Co).

2. INTENTIONAL TRANSFORMATION

In this section, we will explore the intentional transformation of transition metal X-ides through anodic and cathodic electrochemical activation processes. Notably, researchers employ these electrochemical activations to enhance the alkaline HER activity of metal X-ides. We will review three types of transformations: oxidation, X-ide-to-another X-ide conversion, and reduction, providing representative examples for each.

2.1. Oxidation of Metal X-ide into Metal Oxide/Hydroxide. In general, alkaline HER ($2H_2O + 2e^- \rightarrow H_2 + 2OH^-$) faces kinetic challenges due to the extra water dissociation step(s) to form H* intermediate species (too-weak OH binding case: $H_2O + * + e^- \rightarrow H^* + OH^-$; too-strong OH binding case: $H_2O + 2* + e^- \rightarrow H^* + OH^* + e^- \rightarrow H^* + * + OH^-$),[86] requiring high overpotentials.[87,88] Pt catalysts work well for acidic HER but are inefficient for alkaline HER due to inactivity with respect to the water dissociation step.[89,90,86] To overcome this inactivity, integrating different materials in nanostructures (i.e., heterostructures) can promote synergistic effects and electron transfer.[90] For example, Pt/metal (oxy)hydroxide heterostructures (e.g., Pt/MO_xH_y, M = Ni, Co) enhance alkaline HER by facilitating water dissociation through hydroxide anions.[91] Transition metal (hydr)oxide/transition metal X-ide composites offer a cost-effective alternative in which the metal X-ide aids in H* formation and ligand exchange.[87] These composites, fabricated through various electrochemical activation [partial surface electrooxidation (or ultrathin (hydr)oxide formation)] methods such as anodic CV[44] and cathodic LSV,[37,38] have demonstrated high alkaline HER activity comparable to Pt/MO_xH_y. As seen in Figure 6a, Ren et al. fabricated heterostructures of nickel nitrides and nickel hydr(oxy)oxide on Ni foam [Ni_3N−$Ni(OH)_2$/NF] by subjecting a Ni_3N sample, precedently prepared on Ni foam (Ni_3N/NF) through nickel metal electrodeposition followed by nitridation, to five cycles of anodic CV activation.[44] TEM analysis of the Ni_3N−$Ni(OH)_2$/NF revealed the formation of an amorphous ultrathin (∼5 nm) nickel hydr(oxy)oxide species on crystalline Ni_3N surfaces (see Figure 6b). To compare the effectiveness of Ni_3N−$Ni(OH)_2$/NF formed through anodic CV activation, the authors also prepared a $Ni(OH)_2$ and Ni_3N composite [Ni_3N+$Ni(OH)_2$/NF] by electrodepositing nickel hydroxide onto the Ni_3N/NF surface. Ni_3N−$Ni(OH)_2$/NF exhibited superior HER activity compared to Ni_3N/NF and Ni_3N+$Ni(OH)_2$/NF (Figure 6c). This enhancement can be attributed to the *in situ* formation of $Ni(OH)_2$ species, which promoted closer assembly and stronger electronic interaction with Ni_3N (as confirmed by XPS). This interaction likely facilitated electron transfer from oxygen sites in $Ni(OH)_2$ to nickel sites in Ni_3N, optimizing the adsorption of water molecules and H* intermediates on the Ni_3N surface. Additionally, Shang et al. conducted cathodic LSV activation to induce partial surface oxidation of vanadium-doped nickel sulfide (Ni_xV_yS).[38] This process successfully produced a bimetallic oxide/sulfide surface (Ni−V oxide/Ni−V sulfide), establishing a dual-site catalytic system that significantly enhanced the HER activity [i.e., HER overpotential (η_{10}) decrease: ∼ 313 → 150 mV].

In addition to employing the heterostructure strategy, the Che group also accomplished partial substitution of sulfur with oxygen in nickel sulfide (Ni_3S_2) through cathodic CA activation (at −0.3 V vs RHE) of varying durations (5 to 50 h),[43] which is unique. This approach ended up forming a $Ni_3S_{2-x}O_x$ catalyst with a nanosheets/microspheres structure with low crystallinity, demonstrating improved intrinsic HER activity and increased surface area (active site number increase). Specifically, after 25 h, the activated sample showed the highest HER activity (η_{10} = 169 mV), which is much higher than the pristine Ni_3S_2 sample (η_{10} = 288 mV). This example questions whether varying electrochemical activation techniques—such as "cathodic versus anodic" and "potentiodynamic versus potentiostatic/galvanostatic"—result in different oxidation behaviors of metal X-ides, an interesting area that merits further exploration.

The anodic/cathodic activation process (e.g., anodic CV[42,35] and anodic-to-cathodic CV[39]) also results in almost complete metal X-ide surface oxidation (rather than partial surface oxidation) while also improving HER activity. For example, Noda and co-workers performed accelerated anodic hydroxylation of nickel sulfide (NiS) by anodic CV with different cycle numbers (100 to 5000).[42] All the hydroxylated NiS samples showed lower HER overpotentials than pristine NiS. Postactivation XPS analysis revealed the almost complete oxidation of the NiS surface into amorphous Ni hydroxide and sulfate species (SO_4^{2-}). Similar to NiS, Yang and co-workers reported the nearly complete surface oxidation of amorphous nickel phosphide (Ni−P) likely into nickel phosphates with nickel oxides/hydroxides after two cycles of CV (i.e., activation) with an anodic-to-cathodic region, resulting in higher HER activity compared to the pristine Ni−P.[39] Unlike NiS and Ni−P, as shown by experiments conducted in our lab,[35] nickel nitride (Ni_3N) almost completely loses the nitrogen component from its surface upon anodic CV cycling (after 500 cycles), forming amorphous Ni hydroxide, resulting in improved HER activity. Instead, our group, the Yang group, and the Noda group attributed the increased activity of these metal X-ide-derived samples to relatively higher surface areas and the amorphous nature of the metal oxide/hydroxide formed during the electrochemical activation. However, the contributions of "bulk" metal X-ide that remains underneath amorphous metal hydroxide and oxyanion species (e.g., SO_4^{2-}, PO_4^{3-}) toward HER activity are still unknown. Additionally, when comparing HER activity among various activated metal X-ides, one may need to consider the impact of "initial" chemical compositions on the resultant structural properties of amorphous metal hydroxides (e.g., nanoporosity).[23,92] Furthermore, in both partial and complete surface oxidation scenarios, it may be necessary to account for the *in situ* reduction of surface metal oxide/hydroxide to its metallic form under HER potentials (refer to Figure 3 and the related discussion in Section 1.2).

2.2. Transformation of Metal X-ide into Another Metal X-ide. In this group, only cathodic activation has been observed to our knowledge.[33,41] During this activation process, the initial transition metal X-ide is converted into a different metal X-ide with enhanced intrinsic HER activity, accompanied by the dissolution of X-ogen. Wang and co-workers used a cathodic LSV activation approach (potential window: −0.8 to −1.6 V vs Hg/HgO; scan speed: 5 mV·s^{-1}) and reported a phase transformation from hexagonal $Ni_{0.85}Se$ to both hexagonal NiSe and rhombohedral Ni_3Se_2 (Figure 6d).[33] This transformation enhanced the HER activity, with optimal performance observed after approximately 300 LSV scans (Figure 6e). This activation process also led to the formation of a NiSe@Ni_3Se_2 core@shell structure, wherein the core consisted of less-crystalline NiSe, and the surface was covered with short-range ordered Ni_3Se_2, resulting from the leaching of Se species. This core@shell structure has been confirmed through various analyses, including TEM (Figures 6f and g) and EDX (Figures 6h and i). Moreover, electron paramagnetic resonance measurements (not depicted here) confirmed that the activation process led to an increased formation of selenium vacancies in the electrocatalyst. This likely optimized its electronic structure, enhancing its alkaline HER efficiency. Notably, during or after the transformation of metal X-ide to another metal X-ide, selenide-based heterostructure surfaces can form, leading to enhanced HER activity. Recently, Zhang and colleagues synthesized $NiSe_2/Ni_{0.85}Se$ heterostructures using hydrothermal synthesis followed by an etching treatment.[41] The optimal $NiSe_2/Ni_{0.85}Se$ heterostructure demonstrated significantly higher HER activity (η_{10} = 76 mV) compared to individual $NiSe_2$ (202 mV) and $Ni_{0.85}Se$ (213 mV). XPS analysis and DFT calculations revealed that, in the $NiSe_2/Ni_{0.85}Se$ composite, electron transfer from $NiSe_2$ to $Ni_{0.85}Se$ led to an increased charge state of $Ni_{0.85}Se$. This elevated charge state allowed $Ni_{0.85}Se$ to supply additional electrons for bonding with protons (H^+), optimizing the Gibbs free energy for H* intermediate adsorption and accelerating the HER kinetics. Incidentally, the authors employed the same LSV activation method used by Wang and colleagues[33] on the $NiSe_2/Ni_{0.85}Se$ composite and analyzed its transformation through XRD. After 500 LSV scans, the diffraction peaks corresponding to $NiSe_2$ vanished, while those of $Ni_{0.85}Se$ remained, suggesting that the $NiSe_2/Ni_{0.85}Se$ composite had transformed into $Ni_{0.85}Se$ (the report did not provide the postactivation HER activity). Nevertheless, this approach also appears to be applicable to other metal X-ides with high X-ogen-to-metal ratios. Future research in this area would be highly valuable.

2.3. Transformation of Metal X-ide into Metal. Researchers have also employed cathodic activation to convert metal X-ides into pure metal forms, enhancing their HER activity.[36,40] The study by Ma et al. revealed that both cathodic CV (Figure 6j) and CP can activate NiS_2 nanosheets grown on Ni foam (NiS_2/NF), leading to HER activity improvement.[36] After approximately 5 h of cathodic CP at −20 mA·cm^{-2}, NiS_2/NF was fully activated. The activated NiS_2/NF (A-NiS_2/NF) exhibited a significantly lower HER overpotential (η_{10}) of 67 mV at −10 mA·cm^{-2} compared to the unactivated NiS_2/NF (122 mV) in 1 M KOH. As shown in the inset of Figure 6j, numerous small nanosheets derived from the original NiS_2 formed after activation, indicating that the cathodic current induced the bulk transformation from NiS_2 to Ni. Notably, XRD and Raman spectroscopy results showed that the diffraction peaks and vibrational signals associated with NiS_2 disappeared after the activation. As illustrated in Figures 6k and l, *in situ* XAS, XANES, and EXAFS analyses revealed that the activated electrocatalyst was composed primarily of metallic Ni (the active species for the HER), with only trace amounts of sulfide remaining. The authors proposed that the small amount of S^{2-} on the metallic Ni serves as an anchor, attracting hydrated cations to the metallic Ni surface through electrostatic and van der Waals forces. This interaction is thought to enhance the kinetically challenging water dissociation step and facilitate the migration of H* intermediates on the Ni surface, thereby improving H_2 production efficiency. Moreover, it was also found that the metallic Ni nanosheets were readily oxidized to ultrathin $Ni(OH)_2$ upon exposure to air. Similar post-HER oxidation was also observed on the cathodic CP-activated $Ni_3Se_4/NiSe_2$ composite. Guo et al. found that $Ni_3Se_4/NiSe_2$ heterostructures on Ni foam can show HER activity improvement through cathodic CP activation (Figures 6m and n).[40] Over a period of approximately 3000 s of CP at −250 mA·cm^{-2}, the $NiSe_2$ component within the $Ni_3Se_4/NiSe_2$ composite underwent dissolution (as shown in the inset of Figure 6m) and reduction, leading to the formation of a Ni_3Se_4/Ni composite, as confirmed by XRD and XPS analyses. Note that before the post-HER XPS measurement, the authors encapsulated the sample in inert gases right after the CP activation to prevent surface oxidation. As explained in Section 1.4, this selective dissolution and reduction occurred because $NiSe_2$ has thermodynamically lower stability than Ni_3Se_4. As depicted in Figure 6n, the resulting Ni_3Se_4/Ni composite demonstrated higher HER current densities, normalized to the electrochemically active surface area (ECSA), than the original Ni_3Se_4/$NiSe_2$ composite, highlighting the superior intrinsic HER activity of the Ni_3Se_4/Ni. DFT calculations also confirmed that the Ni_3Se_4/Ni heterostructure achieves more moderate hydrogen adsorption and higher HER activity compared to Ni_3Se_4 or Ni individually. The authors performed XPS analysis on the activated sample (Ni_3Se_4/Ni) without inert gas protection to investigate the effects of post-HER oxidation. In the absence of protection, Ni^0 species were no longer detectable, while SeO_2 species emerged. Moreover, the intensity of the characteristic NiO peak increased significantly. These findings led the authors to conclude that the formation of surface NiO and SeO_2 is associated with post-HER oxidation upon exposure to air. As discussed in Sections 1.2 and 1.4, to minimize or ignore the effects of post-HER oxidation and more accurately identify the real HER active species, it is essential to conduct *in situ* characterizations rather than *ex situ* ones in future studies. Alternatively, accurate *ex situ* characterizations require meticulous attention,[40] as noted above.

3. CRYSTALLINITY ALTERNATION

In addition to changes in chemical composition, we observe a distinct phenomenon: the alteration of crystallinity in metal X-ides under applied potential/current (see Figure 7a). For example, Chang et al. used two CV cycles with a potential window of 0.6 to −1.3 V vs Ag/AgCl on amorphous nickel phosphide coated on stainless steel mesh (Ni−P/SSM) (Figure 7b).[39] This process resulted in the formation of crystalline nickel phosphide (Ni_5P_4) nanoparticles, approximately 3 nm in diameter, embedded within an amorphous matrix (likely nickel phosphate and oxides/hydroxides), as shown in Figure 7c. After this transformation, the CV-treated Ni−P/SSM exhibited a reduced HER overpotential (η_{10}) of 87 mV at −10 mA·cm^{-2} and a higher double-layer capacitance (C_{dl}) of 0.372 mF·cm^{-2} compared to the pristine Ni−P/SSM (η_{10}: 104 mV; C_{dl}: 0.151 mF·cm^{-2}). The authors attributed the improved HER activity to the Ni_5P_4 nanoparticles. However, as discussed in Section 2.1, the contribution of these nanoparticles is uncertain since they appear to be fully covered by amorphous species (see Figure 7c). Furthermore, it remains unclear whether the observed HER activity is primarily due to increased surface area rather than the formation of crystalline nickel phosphides. Anantharaj et al. noted a similar crystallization effect in nickel sulfide.[42] Specifically, anodic CV activation of NiS on Ni foam (Ni−S−OH/Ni foam) followed by over 50 h of CA at −0.32 and −0.40 V vs RHE resulted in the appearance of diffraction peaks corresponding to NiS and Ni_3S_2, indicating the growth of these crystalline phases (Figures 7d and e). Nonetheless, similar to the nickel phosphide example, the impact of crystalline NiS and Ni_3S_2 on HER activity remains unclear. Therefore, a more rigorous examination of how crystallinity in metal X-ides affects HER activity and stability is needed to gain further insight into the performance of these electrocatalysts. Recently, Zhao et al. conducted a study examining the impact of electrocatalyst crystallinity on alkaline HER performance.[93] They synthesized porous ruthenium selenides ($RuSe_2$) with varying crystallinities using a combination of hydrothermal synthesis and post-annealing treatment. DFT calculations revealed that amorphous $RuSe_2$ modulates the binding strength for water molecules, while crystalline $RuSe_2$ exhibits optimal hydrogen intermediate binding energy (ΔG_{H*}). This suggests that a hybrid of amorphous and crystalline $RuSe_2$ could serve as an ideal electrocatalyst for alkaline HER. Experimentally, the hybrid $RuSe_2$ outperformed both its highly crystalline (η_{10}: 87 mV) and amorphous (η_{10}: 156 mV) counterparts, achieving better HER activity with an overpotential of 27 mV at −10 mA·cm^{-2}. This study highlights the potential to fine-tune the properties of metal X-ide electrocatalysts by modulating their crystallinity, warranting further investigation in the future.

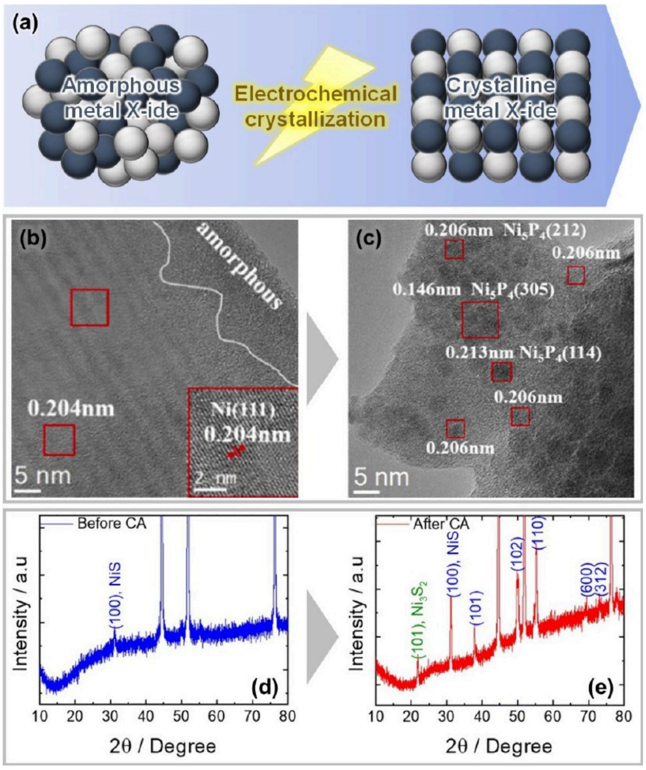

Figure 7. (a) Schematic illustration of electrochemical deamorphization (crystallization) of amorphous metal X-ides. TEM images of amorphous nickel phosphide on stainless steel mesh (Ni−P/SSM) (b) before and (c) after the cathodic CV activation. Reprinted with permission from ref 39. Copyright 2022 Elsevier. XRD patterns of anodic CV-activated NiS on Ni foam (Ni−S−OH/Ni foam) (d) before and (e) after long-term HER testing (more than 50 h of CA). Reprinted with permission from ref 42. Copyright 2020 Elsevier.

4. THERMODYNAMICS AND KINETICS OF PHASE TRANSFORMATION

In this section, we begin by reviewing the thermodynamic and kinetic aspects essential for understanding the phase transformation of transition metal X-ides at various stages of HER testing in alkaline media. We attempt to propose a generalized model for the transformation behavior of metal X-ides as alkaline HER electrocatalysts and to highlight a few key challenges in this field. Thermodynamics provides electrochemists with insights into phase transformation tendencies under given conditions. Specifically, the potential−pH (Pourbaix) diagram serves as an invaluable and practical tool.[94,95] As used in earlier sections, Pourbaix diagrams can provide equilibrium conditions, offering a roadmap of thermodynamically feasible phases and transformations. Currently, one of the most user-friendly and comprehensive databases is the Materials Project, which provides access to computationally (DFT) generated Pourbaix diagrams for a wide range of metal X-ides and other compounds. This resource enables electrochemists to readily predict metal X-ide stability under specific conditions, such as applied potentials and electrolyte pH. However, it is important to note that the Materials Project Pourbaix diagrams, generated using the Perdew−Burke−Ernzerhof functional,[96] may not always accurately predict stability (e.g., in cases such as MoS_2, SeO_2), as highlighted by the Nørskov group.[29,97] The Nørskov group also recommends using the strongly constrained and appropriately normed functional to generate more accurate Pourbaix diagrams.[29,97] Despite their utility, DFT-based Pourbaix diagrams remain limited to thermodynamic predictions, excluding kinetic factors, and thus still require experimental validation. Additionally, other thermodynamic parameters, such as the enthalpies of formation of metal X-ides, can provide valuable insights into stability trends, which we recommend readers consider.[19,98−100]

On the other hand, when discussing kinetics, our focus is on the rates of the phase transformation reactions of metal X-ides under alkaline media. Generally, within the potential range that indicates a thermodynamic tendency for transformation, the rates of anodic and cathodic phase transformation reactions can increase as the potential rises anodically and cathodically, respectively. However, the newly formed surface solid phases, such as metal oxide/hydroxide, X-ogen-poor metal X-ide, pure metal, and elemental X-ogen, significantly influence the kinetics of the phase transformation process.[94] These surface solid phases can be a protective layer that acts as a barrier, hindering interaction between the metal X-ide surface and the alkaline electrolyte. As a result, this protective layer can significantly reduce the rate of phase transformation, even when thermodynamic considerations indicate that active phase transformation should occur. Furthermore, the nature of the protective layer, such as its porosity, thickness, and surface coverage, can influence the degree of metal X-ide and electrolyte interaction, further altering the rate of the phase transformation reaction. Notably, it is known that the nature of the protective layer can vary depending on the electrochemical techniques (e.g., CV and CP) used for OER testing.[25] A similar trend may occur for the HER, highlighting the need for future study in this area. Additionally, the rate of phase transformation per unit projected area (i.e., current density) is affected by the electrocatalyst morphology, a surface area-determining factor, adding another layer of complexity. These factors present substantial challenges in fully understanding the behavior of metal X-ides as alkaline HER electrocatalysts.

Building on the discussions in previous sections, we propose a generic model for the transformation behavior of metal X-ides as alkaline HER electrocatalysts (see Figure S9). As previously noted, metal X-ides can undergo transitions into three distinct phases: metal oxides/hydroxides, metals, and metal X-ides with a reduced X element-to-metal ratio. As illustrated in Figure S9, *in situ* X-ide-to-X-ide conversion and X-ide-to-metal reduction occur during HER testing. In contrast, the formation of metal oxide/hydroxide from metal X-ide or *in situ* formed metal takes place mostly before and/or after HER testing due to oxidation in a strong alkaline medium at OCP or through instantaneous aerial oxidation upon removal from the electrolyte.[40,82,83] Note that these surface metal oxide/hydroxide species can be partially or fully reduced back to metal by reapplying highly cathodic HER potentials.[77−79,101] We further suggest the intriguing possibility that, under harsh HER conditions (i.e., industrial-relevant conditions), many metal X-ides may be fully converted into metals on their surfaces and/or in their bulk, with X element-deficient X-ides as intermediates and metals as the true active species.

> We further suggest the intriguing possibility that, under harsh HER conditions (i.e., industrial-relevant conditions), many metal X-ides may be fully converted into metals on their surfaces and/or in their bulk, with X element-deficient X-ides as intermediates and metals as the true active species.

Finally, we highlight several factors that future studies should consider when investigating the transformation of metal X-ides as electrocatalysts for alkaline HER. Phase transformation heterogeneity is crucial, especially for crystalline metal X-ide electrocatalysts. For instance, our group examined phase and morphological transformations in cubic V_8C_7 under alkaline OER conditions, revealing that its (100), (010), and (001) surfaces were more stable than the (110) and (111) surfaces.[102] More recently, the Moreno-Hernandez group used liquid-phase TEM to demonstrate that RuO_2 nanocrystals exhibit varying stability across different low-index crystal facets, indicated by differing dissolution rates along specific directions in acidic media.[103] These examples underscore that electrocatalyst stability strongly depends on exposed crystal facets, an area that warrants further investigation in metal X-ide electrocatalysts for alkaline HER. Additionally, researchers should be aware that different electrochemical techniques (e.g., CV, CP, CA) used in long-term HER testing may result in varying phase transformations, even for the same material. Wu et al. employed two electrochemical techniques: multiscan LSV and CA, along with XRD, to examine phase transformations in the $NiSe_2/Ni_{0.85}Se$ composite under alkaline conditions.[41] Following 500 LSV scans (potential range: − 0.8 to −1.6 V vs Hg/HgO; scan rate: 5 $mV \cdot s^{-1}$), the $NiSe_2/Ni_{0.85}Se$ composite converted to entirely $Ni_{0.85}Se$. However, after 100 h of CA (applied potential: − 0.076 V vs RHE), the composite bulk remained stable, retaining its original $NiSe_2/Ni_{0.85}Se$ phase. As discussed earlier, metal X-ides often convert into their metallic forms under highly cathodic potentials during the HER process. In other words, increasing cathodic potential may promote leaching of the X-ogen. Future studies could explore the potential- and time-dependent HER stability of metal X-ides in alkaline media, providing further insights.

5. SUMMARY AND OUTLOOK

In this Focus Review, we collectively explored the electrocatalytic behaviors of transition metal X-ides for alkaline HER. We investigated both incidental and intentional transformations of these metal X-ides, discussing their surface HER active species and classifying them into four categories: "no transformation," "X-ide to oxide/hydroxide," "X-ide to metal," and "X-ide to another X-ide." It was found that most of the metal X-ides reported so far undergo some form of phase or structural change during the HER. Extrapolating further, we would anticipate that under highly cathodic HER potentials [i.e., industrial-relevant conditions (current density: 2 A·cm^{-2}; cell voltage: 1.7 V; etc.)],[5] most of the metal X-ide precatalysts for alkaline HER will eventually be transformed into pure metal species on their surfaces and/or in their bulk.

We also underscored the essential need for thorough material characterization before, during (*in situ*), and after HER testing to accurately assess the stability and electrocatalytically active phases of these materials.

We also underscored the essential need for thorough material characterization before, during (*in situ*), and after HER testing to accurately assess the stability and electrocatalytically active phases of these materials. Additionally, we offer general requirements, recommendations, and precautions for characterizing metal X-ides as alkaline HER electrocatalysts, outlined below:

- *In situ* characterization techniques [e.g., *in situ* synchrotron XRD,[45] *in situ* XPS,[104] *in situ* XAS/XANES/EXAFS,[36,67,83] *in situ* (S)TEM,[32,83] *in situ* Raman spectroscopy,[40,41,45,76−79,81−83,104] online ICP-MS,[105] quasi-*in situ* SEM/EDX,[102] etc.] are essential for detecting HER active species (e.g., transition metal species) with relatively short lifetimes without applied HER potentials.
- Researchers should investigate how oxyanions leached *in situ* from metal X-ides into the electrolyte affect the HER activity and stability.
- Researchers must consider pre- and post-HER oxidation of metal X-ides and its impact on HER performance.
- For *ex situ* characterization, special precautions should be taken to prevent post-HER surface reactions, such as chemical oxidation by alkaline media or atmospheric oxygen.[40]
- Researchers can use online databases like the Materials Project to predict the stability of target metal X-ides under HER conditions.
- Pourbaix diagrams are effective for evaluating a material's thermodynamic stability but do not offer insights into the kinetics of transformation reactions, such as side reactions (e.g., oxidation/reduction) or dissolution. To understand reaction kinetics thoroughly, both *ex situ* and *in situ* analyses of electrocatalysts and electrolytes should be performed.
- The impact of X-ogen species (e.g., SO_4^{2-}, PO_4^{3-}, S^{2-}, etc.), generated during phase transformation, on HER performance requires thorough investigation.

Finally, we hope this study will advance future research focused on the transformation behaviors of metal X-ides and aid in identifying their catalytically active species, thereby providing insights for designing efficient, earth-abundant electrocatalysts for alkaline HER.

■ ASSOCIATED CONTENT

Supporting Information

The Supporting Information is available free of charge at https://pubs.acs.org/doi/10.1021/acsenergylett.4c02182.

Pourbaix diagrams for Ni_3P, CoSe, ZnSe, $Ni(OH)_2$, $Co(OH)_2$, CuO, Ni_3S_2 and NiSe in aqueous solutions, and a schematic illustration of the transformation mechanism of transition metal X-ides as HER electrocatalysts in alkaline media. (PDF)

■ AUTHOR INFORMATION

Corresponding Author

C. Buddie Mullins − *Department of Chemistry, The University of Texas at Austin, Austin, Texas 78712, United States; McKetta Department of Chemical Engineering, Center for Electrochemistry, Texas Materials Institute, and H2@UT, The University of Texas at Austin, Austin, Texas 78712, United States;* orcid.org/0000-0003-1030-4801; Email: mullins@che.utexas.edu

Authors

Kenta Kawashima − *Department of Chemistry, The University of Texas at Austin, Austin, Texas 78712, United States;* orcid.org/0000-0001-7318-6115

Antony Elvin Fernando Milton − *Department of Chemistry, The University of Texas at Austin, Austin, Texas 78712, United States;* orcid.org/0009-0004-0826-8869

John S. Archer − *McKetta Department of Chemical Engineering, The University of Texas at Austin, Austin, Texas 78712, United States;* orcid.org/0009-0001-0767-7618

Daniel T. Collins − *McKetta Department of Chemical Engineering, The University of Texas at Austin, Austin, Texas 78712, United States;* orcid.org/0009-0000-8017-9917

Nicolas Lorenzo Serrat − *Department of Chemistry, The University of Texas at Austin, Austin, Texas 78712, United States;* orcid.org/0009-0000-5657-4685

Chikaodili E. Chukwuneke − *Department of Chemistry, The University of Texas at Austin, Austin, Texas 78712, United States;* orcid.org/0000-0003-0478-8387

Raul A. Marquez − *Department of Chemistry, The University of Texas at Austin, Austin, Texas 78712, United States;* orcid.org/0000-0003-3885-5007

Lettie A. Smith − *Department of Chemistry, The University of Texas at Austin, Austin, Texas 78712, United States;* orcid.org/0000-0003-0378-072X

Complete contact information is available at: https://pubs.acs.org/10.1021/acsenergylett.4c02182

Notes

The authors declare no competing financial interest.

Biographies

Kenta Kawashima received his B.Eng. (2014) and M.Eng. (2016) from Shinshu University. He is currently a Ph.D. candidate (Chemistry) at the University of Texas at Austin. His research focuses on developing (photo)electrocatalysts for efficient water splitting and exploring the application of a molten-salt synthesis method for studying crystal growth.

Antony Elvin Fernando Milton is currently a junior Dean's Scholar in B.S. Chemistry (Honors) at the University of Texas at Austin and will graduate in Spring 2026. Planning to pursue a Ph.D. in Chemistry, he leads undergraduate research under Kenta Kawashima, focusing on sustainable materials and electrochemistry applications.

John S. Archer is currently an undergraduate student at the University of Texas at Austin studying Chemical Engineering with focuses in materials engineering and process and systems engineering.

He is serving as an undergraduate researcher in Prof. C. Buddie Mullins' laboratory. His research interests include electrocatalysis for water splitting and electrode synthesis.

Daniel T. Collins is currently working towards his B.S. in Chemical Engineering (2026) from the University of Texas at Austin. His interests involve the development of electrocatalysts, surface chemistry, and their applications to the OER and HER.

Nicolas Lorenzo Serrat is an undergraduate at the University of Texas at Austin, currently pursuing a B.S. in Chemistry (2024). His research focuses on the development of efficient electrocatalysts for water splitting.

Chikaodili E. Chukwuneke received his B.Sc. in Petroleum Chemistry (2014) from the American University of Nigeria. He is currently a Ph.D. candidate (Chemistry) at the University of Texas at Austin. His research applies nature's principles to design advanced electrocatalysts for water splitting and uses analytical chemistry to investigate their properties.

Raul A. Marquez received his B.E. in Chemical Engineering (2017) and M.S. in Chemistry (2020) from Universidad Autonoma de Chihuahua, Mexico. He is a Chemistry Ph.D. candidate at the University of Texas at Austin, researching electrocatalysis, analytical chemistry, and electrochemical engineering, with a focus on energy storage and conversion technologies.

Lettie A. Smith received her B.S. in Chemistry from the University of North Carolina at Chapel Hill in Spring 2020. She began graduate school at the University of Texas at Austin in Fall 2020 under the supervision of Prof. C. Buddie Mullins. Her research focuses on electrocatalysis for the ORR, HER, and OER.

C. Buddie Mullins received a Ph.D. from the California Institute of Technology and was a postdoc at IBM Almaden Research Center. He is a Professor in the Departments of Chemical Engineering and Chemistry at the University of Texas at Austin. His interests include surface chemistry, electrocatalysis, batteries, and CO_2 capture.

■ ACKNOWLEDGMENTS

The authors gratefully acknowledge the support of the National Science Foundation via Grant CHE-2102307.

■ REFERENCES

(1) Turner, J. A. Sustainable Hydrogen Production. *Science* **2004**, *305* (5686), 972−974.

(2) Davis, S. J.; Lewis, N. S.; Shaner, M.; Aggarwal, S.; Arent, D.; Azevedo, I. L.; Benson, S. M.; Bradley, T.; Brouwer, J.; Chiang, Y.-M.; Clack, C. T. M.; Cohen, A.; Doig, S.; Edmonds, J.; Fennell, P.; Field, C. B.; Hannegan, B.; Hodge, B.-M.; Hoffert, M. I.; Ingersoll, E.; Jaramillo, P.; Lackner, K. S.; Mach, K. J.; Mastrandrea, M.; Ogden, J.; Peterson, P. F.; Sanchez, D. L.; Sperling, D.; Stagner, J.; Trancik, J. E.; Yang, C.-J.; Caldeira, K. Net-Zero Emissions Energy Systems. *Science* **2018**, *360* (6396), No. eaas9793.

(3) Bourzac, K. US Hands Out $7 Billion for Hydrogen Hubs. *Science* **2023**, *382* (6668), 253−253.

(4) *Technical Targets for Proton Exchange Membrane Electrolysis*. Energy.gov. https://www.energy.gov/eere/fuelcells/technical-targets-proton-exchange-membrane-electrolysis (accessed 2024-05-02).

(5) *Technical Targets for Liquid Alkaline Electrolysis*. Energy.gov. https://www.energy.gov/eere/fuelcells/technical-targets-liquid-alkaline-electrolysis (accessed 2024-01-11).

(6) *Technical Targets for High Temperature Electrolysis*. Energy.gov. https://www.energy.gov/eere/fuelcells/technical-targets-high-temperature-electrolysis (accessed 2024-05-02).

(7) Kou, T.; Wang, S.; Li, Y. Perspective on High-Rate Alkaline Water Splitting. *ACS Mater. Lett.* **2021**, *3* (2), 224−234.

(8) Ehlers, J. C.; Feidenhans'l, A. A.; Therkildsen, K. T.; Larrazábal, G. O. Affordable Green Hydrogen from Alkaline Water Electrolysis: Key Research Needs from an Industrial Perspective. *ACS Energy Lett.* **2023**, *8* (3), 1502−1509.

(9) Marquez, R. A.; Espinosa, M.; Kalokowski, E.; Son, Y. J.; Kawashima, K.; Le, T. V.; Chukwuneke, C. E.; Mullins, C. B. A Guide to Electrocatalyst Stability Using Lab-Scale Alkaline Water Electrolyzers. *ACS Energy Lett.* **2024**, *9* (2), 547−555.

(10) Guo, Y.; Li, G.; Zhou, J.; Liu, Y. Comparison between Hydrogen Production by Alkaline Water Electrolysis and Hydrogen Production by PEM Electrolysis. *IOP Conf. Ser. Earth Environ. Sci.* **2019**, *371* (4), 042022.

(11) Zeng, K.; Zhang, D. Recent Progress in Alkaline Water Electrolysis for Hydrogen Production and Applications. *Prog. Energy Combust. Sci.* **2010**, *36* (3), 307−326.

(12) Manabe, A.; Kashiwase, M.; Hashimoto, T.; Hayashida, T.; Kato, A.; Hirao, K.; Shimomura, I.; Nagashima, I. Basic Study of Alkaline Water Electrolysis. *Electrochim. Acta* **2013**, *100*, 249−256.

(13) Anantharaj, S.; Ede, S. R.; Sakthikumar, K.; Karthick, K.; Mishra, S.; Kundu, S. Recent Trends and Perspectives in Electrochemical Water Splitting with an Emphasis on Sulfide, Selenide, and Phosphide Catalysts of Fe, Co, and Ni: A Review. *ACS Catal.* **2016**, *6* (12), 8069−8097.

(14) Anantharaj, S.; Kundu, S.; Noda, S. Progress in Nickel Chalcogenide Electrocatalyzed Hydrogen Evolution Reaction. *J. Mater. Chem. A* **2020**, *8* (8), 4174−4192.

(15) Tang, S.; Zhang, Z.; Xiang, J.; Yang, X.; Shen, X.; Song, F. Recent Advances in Transition Metal Nitrides for Hydrogen Electrocatalysis in Alkaline Media: From Catalyst Design to Application.*Front. Chem.* **2022**, *10*,1073175 .

(16) Feidenhans'l, A. A.; Regmi, Y. N.; Wei, C.; Xia, D.; Kibsgaard, J.; King, L. A. Precious Metal Free Hydrogen Evolution Catalyst Design and Application. *Chem. Rev.* **2024**, *124* (9), 5617−5667.

(17) Wygant, B. R.; Kawashima, K.; Mullins, C. B. Catalyst or Precatalyst? The Effect of Oxidation on Transition Metal Carbide, Pnictide, and Chalcogenide Oxygen Evolution Catalysts. *ACS Energy Lett.* **2018**, *3* (12), 2956−2966.

(18) Ding, H.; Liu, H.; Chu, W.; Wu, C.; Xie, Y. Structural Transformation of Heterogeneous Materials for Electrocatalytic Oxygen Evolution Reaction. *Chem. Rev.* **2021**, *121* (21), 13174−13212.

(19) Kawashima, K.; Márquez, R. A.; Smith, L. A.; Vaidyula, R. R.; Carrasco-Jaim, O. A.; Wang, Z.; Son, Y. J.; Cao, C. L.; Mullins, C. B. A Review of Transition Metal Boride, Carbide, Pnictide, and Chalcogenide Water Oxidation Electrocatalysts. *Chem. Rev.* **2023**, *123* (23), 12795−13208.

(20) Zhu, J.; Hu, L.; Zhao, P.; Lee, L. Y. S.; Wong, K.-Y. Recent Advances in Electrocatalytic Hydrogen Evolution Using Nanoparticles. *Chem. Rev.* **2020**, *120* (2), 851−918.

(21) Bellato, F.; Ferri, M.; Annamalai, A.; Prato, M.; Leoncino, L.; Brescia, R.; De Trizio, L.; Manna, L. Colloidal Synthesis of Nickel Arsenide Nanocrystals for Electrochemical Water Splitting. *ACS Appl. Energy Mater.* **2023**, *6* (1), 151−159.

(22) Mabayoje, O.; Shoola, A.; Wygant, B. R.; Mullins, C. B. The Role of Anions in Metal Chalcogenide Oxygen Evolution Catalysis: Electrodeposited Thin Films of Nickel Sulfide as "Pre-Catalysts. *ACS Energy Lett.* **2016**, *1* (1), 195−201.

(23) Kawashima, K.; Márquez-Montes, R. A.; Li, H.; Shin, K.; Cao, C. L.; Vo, K. M.; Son, Y. J.; Wygant, B. R.; Chunangad, A.; Youn, D. H.; Henkelman, G.; Ramos-Sánchez, V. H.; Mullins, C. B. Electrochemical Behavior of a Ni_3N OER Precatalyst in Fe-Purified Alkaline Media: The Impact of Self-Oxidation and Fe Incorporation. *Mater. Adv.* **2021**, *2* (7), 2299−2309.

(24) Marquez-Montes, R. A.; Kawashima, K.; Son, Y. J.; Weeks, J. A.; Sun, H. H.; Celio, H.; Ramos-Sánchez, V. H.; Mullins, C. B. Mass Transport-Enhanced Electrodeposition of Ni-S-P-O Films on Nickel Foam for Electrochemical Water Splitting. *J. Mater. Chem. A* **2021**, *9* (12), 7736−7749.

(25) Son, Y. J.; Kim, S.; Leung, V.; Kawashima, K.; Noh, J.; Kim, K.; Marquez, R. A.; Carrasco-Jaim, O. A.; Smith, L. A.; Celio, H.; Milliron, D. J.; Korgel, B. A.; Mullins, C. B. Effects of Electrochemical Conditioning on Nickel-Based Oxygen Evolution Electrocatalysts. *ACS Catal.* **2022**, *12* (16), 10384−10399.

(26) Jin, S. Are Metal Chalcogenides, Nitrides, and Phosphides Oxygen Evolution Catalysts or Bifunctional Catalysts? *ACS Energy Lett.* **2017**, *2* (8), 1937−1938.

(27) Li, W.; Gao, X.; Xiong, D.; Xia, F.; Liu, J.; Song, W.-G.; Xu, J.; Thalluri, S. M.; Cerqueira, M. F.; Fu, X.; Liu, L. Vapor-Solid Synthesis of Monolithic Single-Crystalline CoP Nanowire Electrodes for Efficient and Robust Water Electrolysis. *Chem. Sci.* **2017**, *8* (4), 2952−2958.

(28) Guo, K.; Li, H.; Huang, J.; Wang, Y.; Peng, Y.; Lu, S.; Xu, C. Selenization Triggers Deep Reconstruction to Produce Ultrathin γ-NiOOH toward the Efficient Water Oxidation. *J. Energy Chem.* **2021**, *63*, 651−658.

(29) Wang, Z.; Zheng, Y.-R.; Montoya, J.; Hochfilzer, D.; Cao, A.; Kibsgaard, J.; Chorkendorff, I.; Nørskov, J. K. Origins of the Instability of Nonprecious Hydrogen Evolution Reaction Catalysts at Open-Circuit Potential. *ACS Energy Lett.* **2021**, *6* (6), 2268−2274.

(30) Huang, J.; Hao, M.; Mao, B.; Zheng, L.; Zhu, J.; Cao, M. The Underlying Molecular Mechanism of Fence Engineering to Break the Activity-Stability Trade-Off in Catalysts for the Hydrogen Evolution Reaction. *Angew. Chem., Int. Ed.* **2022**, *61* (10), No. e202114899.

(31) Du, L.; Zheng, W. Catalyst Deactivation during Water Electrolysis: Understanding and Mitigation. *APL Energy* **2024**, *2* (2), 021501.

(32) Fu, Q.; Wong, L. W.; Zheng, F.; Zheng, X.; Tsang, C. S.; Lai, K. H.; Shen, W.; Ly, T. H.; Deng, Q.; Zhao, J. Unraveling and Leveraging In Situ Surface Amorphization for Enhanced Hydrogen Evolution Reaction in Alkaline Media. *Nat. Commun.* **2023**, *14* (1), 6462.

(33) Jiang, L.-W.; Yin, Z.-H.; Liu, H.; Wang, J.-J. Universal Phase Transformation of Ni-Se Electrocatalysts Induced by an Electrochemical Activation Strategy for a Significantly Enhanced Alkaline Hydrogen Evolution Reaction. *Mater. Chem. Front.* **2023**, *7* (14), 2871−2879.

(34) Kundu, A.; Chakraborty, B. Surface Structure to Tailor the Electrochemical Behavior of Mixed-Valence Copper Sulfides during Water Electrolysis. *JACS Au* **2024**, *4* (2), 642−656.

(35) Chukwuneke, C. E.; Kawashima, K.; Li, H.; Marquez, R. A.; Son, Y. J.; Smith, L. A.; Celio, H.; Henkelman, G.; Mullins, C. B. Electrochemically Engineered Domain: Nickel-Hydroxide/Nickel Nitride Composite for Alkaline HER Electrocatalysis. *J. Mater. Chem. A* **2024**, *12* (3), 1654−1661.

(36) Ma, Q.; Hu, C.; Liu, K.; Hung, S.-F.; Ou, D.; Chen, H. M.; Fu, G.; Zheng, N. Identifying the Electrocatalytic Sites of Nickel Disulfide in Alkaline Hydrogen Evolution Reaction. *Nano Energy* **2017**, *41*, 148−153.

(37) Shang, X.; Yan, K.-L.; Rao, Y.; Dong, B.; Chi, J.-Q.; Liu, Y.-R.; Li, X.; Chai, Y.-M.; Liu, C.-G. *In Situ* Cathodic Activation of V-Incorporated Ni_xS_y Nanowires for Enhanced Hydrogen Evolution. *Nanoscale* **2017**, *9* (34), 12353−12363.

(38) Shang, X.; Zhang, X.-Y.; Xie, J.-Y.; Dong, B.; Chi, J.-Q.; Guo, B.-Y.; Yang, M.; Chai, Y.-M.; Liu, C.-G. Double-Catalytic-Site Engineering of Nickel-Based Electrocatalysts by Group VB Metals Doping Coupling with In-Situ Cathodic Activation for Hydrogen Evolution. *Appl. Catal. B Environ.* **2019**, *258*, 117984.

(39) Chang, X.; Ma, K.; Wu, X.; Deng, R.; Wang, Z.; Yang, H. Enhanced Electrocatalytic Water Splitting by Adjusting the Local Reaction Environment with Nickel Coordination Regulation. *J. Alloys Compd.* **2023**, *938*, 168557.

(40) Guo, K.; Wang, Y.; Huang, J.; Li, H.; Peng, Y.; Xu, C. Symbiotic Ni_3Se_4/Ni Heterostructure Induced by Unstable $NiSe_2$ for Enhanced Hydrogen Generation. *Chem. Eng. J.* **2023**, *454*, 140488.

(41) Wu, K.; Lyu, C.; Cheng, J.; Guo, Z.; Li, H.; Zhu, X.; Lau, W.-M.; Zheng, J. Modulating Electronic Structure by Etching Strategy to Construct $NiSe_2$/$Ni_{0.85}Se$ Heterostructure for Urea-Assisted Hydrogen Evolution Reaction. *Small* **2024**, *20* (9), 2304390.

(42) Anantharaj, S.; Sugime, H.; Noda, S. Surface Amorphized Nickel Hydroxy Sulphide for Efficient Hydrogen Evolution Reaction in Alkaline Medium. *Chem. Eng. J.* **2021**, *408*, 127275.

(43) Hao, S.; Liu, J.; Cao, Q.; Zhao, Y.; Zhao, X.; Pei, K.; Zhang, J.; Chen, G.; Che, R. In-Situ Electrochemical Pretreatment of Hierarchical Ni_3S_2-Based Electrocatalyst towards Promoted Hydrogen Evolution Reaction with Low Overpotential. *J. Colloid Interface Sci.* **2020**, *559*, 282−290.

(44) Ren, J.-T.; Wang, Y.-S.; Song, Y.-J.; Chen, L.; Yuan, Z.-Y. Interface Engineering of In-situ Formed Nickel Hydr(Oxy)Oxides on Nickel Nitrides to Boost Alkaline Hydrogen Electrocatalysis. *Appl. Catal. B Environ.* **2022**, *309*, 121279.

(45) Zhai, L.; Benedict Lo, T. W.; Xu, Z.-L.; Potter, J.; Mo, J.; Guo, X.; Tang, C. C.; Edman Tsang, S. C.; Lau, S. P. *In Situ* Phase Transformation on Nickel-Based Selenides for Enhanced Hydrogen Evolution Reaction in Alkaline Medium. *ACS Energy Lett.* **2020**, *5* (8), 2483−2491.

(46) Li, X.; Zhang, L.; Huang, M.; Wang, S.; Li, X.; Zhu, H. Cobalt and Nickel Selenide Nanowalls Anchored on Graphene as Bifunctional Electrocatalysts for Overall Water Splitting. *J. Mater. Chem. A* **2016**, *4* (38), 14789−14795.

(47) Hu, L.; Zhong, P.; Zhang, X.; Xiang, Y.; Balogun, M.-S.; Tong, Y.; Yang, H. Electronic Modulation of Zinc Selenide toward Efficient Alkaline Hydrogen Evolution. *Appl. Surf. Sci.* **2023**, *623*, 157040.

(48) Wu, H.; Wang, Z.; Li, Z.; Ma, Y.; Ding, F.; Li, F.; Bian, H.; Zhai, Q.; Ren, Y.; Shi, Y.; Yang, Y.; Deng, Y.; Tang, S.; Meng, X. Medium-Entropy Metal Selenides Nanoparticles with Optimized Electronic Structure as High-Performance Bifunctional Electrocatalysts for Overall Water Splitting. *Adv. Energy Mater.* **2023**, *13* (28), 2300837.

(49) Cao, D.; Shao, J.; Cui, Y.; Zhang, L.; Cheng, D. Interfacial Engineering of Copper-Nickel Selenide Nanodendrites for Enhanced Overall Water Splitting in Alkali Condition. *Small* **2023**, *19* (33), 2301613.

(50) Ahmed, M.; Hanan, A.; Lakhan, M. N.; Shar, A. H.; Soomro, I. A.; Niu, B.; Yang, Y. One-Pot Synthesis of Crystalline Structure: Nickel-Iron Phosphide and Selenide for Hydrogen Production in Alkaline Water Splitting: Original Scientific Paper. *J. Electrochem. Sci. Eng.* **2023**, *13* (3), 575−588.

(51) Zhang, Y.; Li, B.; Zhou, A.; Li, D.; Shao, X.; Zhu, L.; Du, Y.; Cao, L.; Yang, J. Fe-Ni-Doped Metal-Organic Framework Derived $CoSe_2$ as an Efficient and Stable Electrocatalyst for Hydrogen Evolution Reaction. *Int. J. Hydrog. Energy* **2024**, *65*, 186−195.

(52) Das, M.; Khan, Z. B.; Kamboj, N.; Banerjee, M.; Dey, R. S. Facile Single Step Electrochemical Growth of Ni_3P on Carbon Cloth for Highly Efficient Hydrogen Evolution Reaction. *J. Electrochem. Soc.* **2022**, *169* (6), 064511.

(53) He, R.; Thangasamy, P.; Wu, J.; Yu, K.; Yu, X.; Tang, W.; Quiroz, D.; Alyones, D.; Chen, Z.; Luo, H.; Zhou, M. Synergistically Coupling of Trimetallic Sulfides on Ni Foam as Porous Self-Supported Electrodes for Alkaline Water Splitting. *Electrochim. Acta* **2023**, *470*, 143342.

(54) Das, M.; Biswas, A.; Khan, Z. B.; Dey, R. S. Tuning the Electronic Structure of Cobalt Selenide on Copper Foam by Introducing a Ni Buffer Layer for Highly Efficient Electrochemical Water Splitting. *Inorg. Chem.* **2022**, *61* (33), 13218−13225.

(55) Cao, J.; Hou, S.; Wang, G.; Yu, W.; Yang, Z.; Wu, Y. Boosting Alkaline/Neutral Hydrogen Evolution Reaction of Nickel Selenium by Introducing Carbon Dopants. *J. Electroanal. Chem.* **2024**, *969*, 118546.

(56) Das, M.; Kumar, G.; Dey, R. S. Electrochemical Growth and Formation Mechanism of Cu_2Se/$CoSe_2$-Based Bifunctional Electrocatalyst: A Strategy for the Development of Efficient Material toward Water Electrolysis. *ACS Appl. Energy Mater.* **2022**, *5* (4), 3915−3925.

(57) Wang, X.; Li, W.; Xiong, D.; Petrovykh, D. Y.; Liu, L. Bifunctional Nickel Phosphide Nanocatalysts Supported on Carbon

Fiber Paper for Highly Efficient and Stable Overall Water Splitting. *Adv. Funct. Mater.* **2016**, *26* (23), 4067−4077.

(58) Panda, C.; Menezes, P. W.; Walter, C.; Yao, S.; Miehlich, M. E.; Gutkin, V.; Meyer, K.; Driess, M. From a Molecular 2Fe-2Se Precursor to a Highly Efficient Iron Diselenide Electrocatalyst for Overall Water Splitting. *Angew. Chem., Int. Ed.* **2017**, *56* (35), 10506−10510.

(59) Menezes, P. W.; Indra, A.; Das, C.; Walter, C.; Göbel, C.; Gutkin, V.; Schmeiβer, D.; Driess, M. Uncovering the Nature of Active Species of Nickel Phosphide Catalysts in High-Performance Electrochemical Overall Water Splitting. *ACS Catal.* **2017**, *7* (1), 103−109.

(60) Zhang, Y.; Gao, L.; Hensen, E. J. M.; Hofmann, J. P. Evaluating the Stability of Co_2P Electrocatalysts in the Hydrogen Evolution Reaction for Both Acidic and Alkaline Electrolytes. *ACS Energy Lett.* **2018**, *3* (6), 1360−1365.

(61) Panda, C.; Menezes, P. W.; Zheng, M.; Orthmann, S.; Driess, M. In Situ Formation of Nanostructured Core-Shell Cu_3N-CuO to Promote Alkaline Water Electrolysis. *ACS Energy Lett.* **2019**, *4* (3), 747−754.

(62) Li, Y.; Wei, B.; Yu, Z.; Bondarchuk, O.; Araujo, A.; Amorim, I.; Zhang, N.; Xu, J.; Neves, I. C.; Liu, L. Bifunctional Porous Cobalt Phosphide Foam for High-Current-Density Alkaline Water Electrolysis with 4000-h Long Stability. *ACS Sustain. Chem. Eng.* **2020**, *8* (27), 10193−10200.

(63) Das, M.; Kamboj, N.; Purkait, T.; Sarkar, S.; Dey, R. S. Revealing the Structural Aspect of Ultrastable Self-Supportive Bifunctional Electrocatalyst for Solar-Driven Water Splitting. *J. Phys. Chem. C* **2020**, *124* (25), 13525−13534.

(64) Fan, K.; Zou, H.; Dharanipragada, N. V. R. A.; Fan, L.; Inge, A. K.; Duan, L.; Zhang, B.; Sun, L. Surface and Bulk Reconstruction of CoW Sulfides during pH-Universal Electrocatalytic Hydrogen Evolution. *J. Mater. Chem. A* **2021**, *9* (18), 11359−11369.

(65) Yang, H.; Guo, P.; Wang, R.; Chen, Z.; Xu, H.; Pan, H.; Sun, D.; Fang, F.; Wu, R. Sequential Phase Conversion-Induced Phosphides Heteronanorod Arrays for Superior Hydrogen Evolution Performance to Pt in Wide pH Media. *Adv. Mater.* **2022**, *34* (20), 2107548.

(66) Das, M.; Khan, Z. B.; Biswas, A.; Dey, R. S. Inter-Electronic Interaction between Ni and Mo in Electrodeposited Ni-Mo-P on 3D Copper Foam Enables Hydrogen Evolution Reaction at Low Overpotential. *Inorg. Chem.* **2022**, *61* (45), 18253−18259.

(67) Peng, W.; Lv, Z.; Zhou, W.; Yan, B.; Zhao, S.; Wu, L.; Zhou, J.; Gou, H. High-Pressure Synthesis of Trimetal Phosphide CFNP as Highly Efficient Bifunctional Catalyst for Alkaline Water Splitting. *Fuel* **2025**, *380*, 133110.

(68) Lu, W.; Li, X.; Wei, F.; Cheng, K.; Li, W.; Zhou, Y.; Zheng, W.; Pan, L.; Zhang, G. In-Situ Transformed Ni, S-Codoped CoO from Amorphous Co-Ni Sulfide as an Efficient Electrocatalyst for Hydrogen Evolution in Alkaline Media. *ACS Sustain. Chem. Eng.* **2019**, *7* (14), 12501−12509.

(69) Jiang, L.-W.; Chen, L.; Wu, Y.-Z.; Liu, H.; Wang, J.-J. Unveiling the Structure Evolution and Regulation of Dynamic Activity and Stability of Co_3Se_4 Electrocatalysts under Alkaline Hydrogen Evolution Reaction with SeO_3^{2-} Ions. *Electrochim. Acta* **2023**, *464*, 142953.

(70) Yang, J.; Liu, H.; Martens, W. N.; Frost, R. L. Synthesis and Characterization of Cobalt Hydroxide, Cobalt Oxyhydroxide, and Cobalt Oxide Nanodiscs. *J. Phys. Chem. C* **2010**, *114* (1), 111−119.

(71) Shi, Y.; Du, W.; Zhou, W.; Wang, C.; Lu, S.; Lu, S.; Zhang, B. Unveiling the Promotion of Surface-Adsorbed Chalcogenate on the Electrocatalytic Oxygen Evolution Reaction. *Angew. Chem., Int. Ed.* **2020**, *59* (50), 22470−22474.

(72) Hausmann, J. N.; Menezes, P. W. Effect of Surface-Adsorbed and Intercalated (Oxy)Anions on the Oxygen Evolution Reaction. *Angew. Chem., Int. Ed.* **2022**, *61* (38), No. e202207279.

(73) Walter, C.; Beltrán-Suito, R.; Schwarze, M.; Gupta, N. K.; Menezes, P. W.; Driess, M. Elemental Chalcogens Acting as Metal-Free Electrocatalysts for Effective Alkaline and Acidic Hydrogen Evolution Reaction. *Catal. Today* **2023**, *423*, 113917.

(74) Hoa, V. H.; Prabhakaran, S.; Le, K. T. N.; Kim, D. H. A Single Atom Ir Doped Heterophase of a $NiMoP$-$NiMoP_xO_y$ Ultrathin Layer Assembled on CNTs-Graphene for High-Performance Water Splitting. *J. Mater. Chem. A* **2022**, *10* (27), 14604−14612.

(75) Hoa, V. H.; Austeria, M.; Thi Dao, H.; Mai, M.; Kim, D. H. Dual-Phase Cobalt Phosphide/Phosphate Hybrid Interactions via Iridium Nanocluster Interfacial Engineering toward Efficient Overall Seawater Splitting. *Appl. Catal. B Environ.* **2023**, *327*, 122467.

(76) Chen, M.; Liu, D.; Chen, Y.; Liu, D.; Du, X.; Feng, J.; Zhou, P.; Zi, B.; Liu, Q.; Lo, K. H.; Chen, S.; Wang, S.; Ip, W. F.; Pan, H. Insightful View on the Active Sites of Ni/Ni_xP for Hydrogen Evolution Reaction. *Appl. Mater. Today* **2022**, *26*, 101343.

(77) Faid, A. Y.; Barnett, A. O.; Seland, F.; Sunde, S. Ni/NiO Nanosheets for Alkaline Hydrogen Evolution Reaction: In Situ Electrochemical-Raman Study. *Electrochim. Acta* **2020**, *361*, 137040.

(78) Lai, W.; Ge, L.; Li, H.; Deng, Y.; Xu, B.; Ouyang, B.; Kan, E. *In Situ* Raman Spectroscopic Study towards the Growth and Excellent HER Catalysis of Ni/$Ni(OH)_2$ Heterostructure. *Int. J. Hydrog. Energy* **2021**, *46* (53), 26861−26872.

(79) Jiang, L.-W.; Huang, Y.; Zou, Y.; Meng, C.; Xiao, Y.; Liu, H.; Wang, J.-J. Boosting the Stability of Oxygen Vacancies in α-$Co(OH)_2$ Nanosheets with Coordination Polyhedrons as Rivets for High-Performance Alkaline Hydrogen Evolution Electrocatalyst. *Adv. Energy Mater.* **2022**, *12* (43), 2202351.

(80) Hall, D. S.; Lockwood, D. J.; Poirier, S.; Bock, C.; MacDougall, B. R. Raman and Infrared Spectroscopy of α and β Phases of Thin Nickel Hydroxide Films Electrochemically Formed on Nickel. *J. Phys. Chem. A* **2012**, *116* (25), 6771−6784.

(81) Sun, Y.; Wu, J.; Zhang, Z.; Liao, Q.; Zhang, S.; Wang, X.; Xie, Y.; Ma, K.; Kang, Z.; Zhang, Y. Phase Reconfiguration of Multivalent Nickel Sulfides in Hydrogen Evolution. *Energy Environ. Sci.* **2022**, *15* (2), 633−644.

(82) Zou, W.; Sun, C.; Zhao, K.; Li, J.; Pan, X.; Ye, D.; Xie, Y.; Xu, W.; Zhao, H.; Zhang, L.; Zhang, J. Surface Reconstruction of NiCoP Pre-Catalysts for Bifunctional Water Splitting in Alkaline Electrolyte. *Electrochim. Acta* **2020**, *345*, 136114.

(83) Zhu, Y.; Chen, H.-C.; Hsu, C.-S.; Lin, T.-S.; Chang, C.-J.; Chang, S.-C.; Tsai, L.-D.; Chen, H. M. Operando Unraveling of the Structural and Chemical Stability of P-Substituted $CoSe_2$ Electrocatalysts toward Hydrogen and Oxygen Evolution Reactions in Alkaline Electrolyte. *ACS Energy Lett.* **2019**, *4* (4), 987−994.

(84) Madadkhani, S.; Nandy, S.; Chae, K. H.; Aleshkevych, P.; Najafpour, M. M. Unraveling the Transformation of Cobalt Sulfide in the Hydrogen Evolution Reaction at a High Overpotential: A Step Toward Deciphering the Mechanism. *ACS Appl. Energy Mater.* **2024**, *7* (1), 165−175.

(85) Madadkhani, S.; Nandy, S.; Chae, K. H.; Aleshkevych, P.; Najafpour, M. M. Unveiling the Changes of Dinickel Phosphide (Ni_2P) in Hydrogen Evolution Reaction: Toward a Deeper Mechanistic Understanding. *ACS Appl. Energy Mater.* **2024**, *7* (8), 3157−3165.

(86) McCrum, I. T.; Koper, M. T. M. The Role of Adsorbed Hydroxide in Hydrogen Evolution Reaction Kinetics on Modified Platinum. *Nat. Energy* **2020**, *5* (11), 891−899.

(87) Anantharaj, S.; Noda, S.; Jothi, V. R.; Yi, S.; Driess, M.; Menezes, P. W. Strategies and Perspectives to Catch the Missing Pieces in Energy-Efficient Hydrogen Evolution Reaction in Alkaline Media. *Angew. Chem., Int. Ed.* **2021**, *60*, 18981.

(88) Chen, Z.; Duan, X.; Wei, W.; Wang, S.; Ni, B.-J. Recent Advances in Transition Metal-Based Electrocatalysts for Alkaline Hydrogen Evolution. *J. Mater. Chem. A* **2019**, *7* (25), 14971−15005.

(89) Sheng, W.; Gasteiger, H. A.; Shao-Horn, Y. Hydrogen Oxidation and Evolution Reaction Kinetics on Platinum: Acid vs Alkaline Electrolytes. *J. Electrochem. Soc.* **2010**, *157* (11), B1529.

(90) Wei, J.; Zhou, M.; Long, A.; Xue, Y.; Liao, H.; Wei, C.; Xu, Z. J. Heterostructured Electrocatalysts for Hydrogen Evolution Reaction Under Alkaline Conditions. *Nano-Micro Lett.* **2018**, *10* (4), 75.

(91) Subbaraman, R.; Tripkovic, D.; Chang, K.-C.; Strmcnik, D.; Paulikas, A. P.; Hirunsit, P.; Chan, M.; Greeley, J.; Stamenkovic, V.; Markovic, N. M. Trends in Activity for the Water Electrolyser Reactions on 3*d* M(Ni,Co,Fe,Mn) Hydr(Oxy)Oxide Catalysts. *Nat. Mater.* **2012**, *11* (6), 550−557.

(92) Kim, J.-H.; Kawashima, K.; Wygant, B. R.; Mabayoje, O.; Liu, Y.; Wang, J. H.; Mullins, C. B. Transformation of a Cobalt Carbide (Co_3C) Oxygen Evolution Precatalyst. *ACS Appl. Energy Mater.* **2018**, *1* (10), 5145−5150.

(93) Zhao, J.; Guo, Y.; Li, S.; Wang, J.; Liu, K.; Dai, L.; Dai, Y.; Jiang, B.; Li, H. Amorphous-Crystalline Porous Ruthenium Selenide as Highly Efficient Electrocatalysts for Alkaline Hydrogen Evolution. *Chem. Eng. J.* **2024**, *485*, 150074.

(94) Kruger, J. Passivity. In *Uhlig's Corrosion Handbook*; John Wiley & Sons, Ltd, 2011; pp 151−155. DOI: 10.1002/9780470872864.ch.

(95) Pourbaix, M. *Atlas of Electrochemical Equilibria in Aqueous Solutions*; National Association of Corrosion Engineers, 1974.

(96) Perdew, J. P.; Burke, K.; Ernzerhof, M. Generalized Gradient Approximation Made Simple. *Phys. Rev. Lett.* **1996**, *77* (18), 3865−3868.

(97) Wang, Z.; Guo, X.; Montoya, J.; Nørskov, J. K. Predicting Aqueous Stability of Solid with Computed Pourbaix Diagram Using SCAN Functional. *npj Comput. Mater.* **2020**, *6* (1), 1−7.

(98) Niessen, A. K.; De Boer, F. R. The Enthalpy of Formation of Solid Borides, Carbides, Nitrides, Silicides and Phosphides of Transition and Noble Metals. *J. Common Met.* **1981**, *82*, 75−80.

(99) Stevanović, V.; Lany, S.; Zhang, X.; Zunger, A. Correcting Density Functional Theory for Accurate Predictions of Compound Enthalpies of Formation: Fitted Elemental-Phase Reference Energies. *Phys. Rev. B* **2012**, *85* (11), 115104.

(100) Rasmussen, F. A.; Thygesen, K. S. Computational 2D Materials Database: Electronic Structure of Transition-Metal Dichalcogenides and Oxides. *J. Phys. Chem. C* **2015**, *119* (23), 13169−13183.

(101) Deng, Y.; Handoko, A. D.; Du, Y.; Xi, S.; Yeo, B. S. *In Situ* Raman Spectroscopy of Copper and Copper Oxide Surfaces during Electrochemical Oxygen Evolution Reaction: Identification of Cu^{III} Oxides as Catalytically Active Species. *ACS Catal.* **2016**, *6* (4), 2473−2481.

(102) Kawashima, K.; Cao, C. L.; Li, H.; Márquez-Montes, R. A.; Wygant, B. R.; Son, Y. J.; Guerrera, J. V.; Henkelman, G.; Mullins, C. B. Evaluation of a V_8C_7 Anode for Oxygen Evolution in Alkaline Media: Unusual Morphological Behavior. *ACS Sustain. Chem. Eng.* **2020**, *8* (37), 14101−14108.

(103) Vigil, S. A.; Moreno-Hernandez, I. A. Dissolution Heterogeneity Observed in Anisotropic Ruthenium Dioxide Nanocrystals via Liquid-Phase Transmission Electron Microscopy. *J. Am. Chem. Soc.* **2024**, *146* (16), 11133−11140.

(104) Liao, L.; Zhou, Q.; Liu, F.; Ma, Y.; Cheng, C.; Huang, H.; Yu, F.; Long, R.; Zhou, H. Deciphering the In Situ Reconstruction of Metal Phosphide/Nitride Dual Heterostructures for Robust Alkaline Hydrogen Evolution Above 3 A cm^{-2}. *Small* **2024**, *20* (29), 2311289.

(105) Escalera-López, D.; Iffelsberger, C.; Zlatar, M.; Novčić, K.; Maselj, N.; Van Pham, C.; Jovanovič, P.; Hodnik, N.; Thiele, S.; Pumera, M.; Cherevko, S. Allotrope-Dependent Activity-Stability Relationships of Molybdenum Sulfide Hydrogen Evolution Electrocatalysts. *Nat. Commun.* **2024**, *15* (1), 3601.